









## Article

# A Facile Synthetic Approach toward Obtaining N-Doped Carbon Quantum Dots from Citric Acid and Amino Acids, and Their Application in Selective Detection of Fe(III) Ions

Silvija Šafranko <sup>1</sup>, Kristina Jandel <sup>2</sup>, Monika Kovačević <sup>2</sup>, Anamarija Stanković <sup>2</sup>, Maja Dutour Sikirić <sup>3</sup>, Šimun Mandić <sup>4</sup>, Aleksandar Széchenyi <sup>5</sup>, Ljubica Glavaš Obrovac <sup>6</sup>, Marijana Leventić <sup>6</sup>, Ivica Strelec <sup>1</sup>, Krunoslav Aladić <sup>1</sup> and Stela Jokić <sup>1,\*</sup>

<sup>1</sup> Faculty of Food Technology Osijek, University of Osijek, Franje Kuhača 18, 31000 Osijek, Croatia

<sup>2</sup> Department of Chemistry, University of Osijek, Ulica cara Hadrijana 8/A, 31000 Osijek, Croatia

<sup>3</sup> Division of Physical Chemistry, Ruđer Bošković Institute, 10000 Zagreb, Croatia

<sup>4</sup> Center of Excellence for Advanced Materials and Sensing Devices, Institute of Physics, Bijenička Cesta 46, 10000 Zagreb, Croatia

<sup>5</sup> Institute of Pharmaceutical Technology and Biopharmacy, Faculty of Pharmacy, University of Pécs, H-7624 Pécs, Hungary

<sup>6</sup> Department of Medical Chemistry, Biochemistry and Clinical Chemistry, University of Osijek, J. Huttlera 4, 31000 Osijek, Croatia

\* Correspondence: sjokic@ptfos.hr; Tel.: +385-31-224-333



**Citation:** Šafranko, S.; Jandel, K.; Kovačević, M.; Stanković, A.; Dutour Sikirić, M.; Mandić, Š.; Széchenyi, A.; Glavaš Obrovac, L.; Leventić, M.; Strelec, I.; et al. A Facile Synthetic Approach toward Obtaining N-Doped Carbon Quantum Dots from Citric Acid and Amino Acids, and Their Application in Selective Detection of Fe(III) Ions. *Chemosensors* **2023**, *11*, 205. <https://doi.org/10.3390/chemosensors11040205>

Academic Editors: Guo-Hui Pan, Hongshang Peng and Biao Dong

Received: 1 February 2023

Revised: 4 March 2023

Accepted: 20 March 2023

Published: 24 March 2023



**Copyright:** © 2023 by the authors. Licensee MDPI, Basel, Switzerland. This article is an open access article distributed under the terms and conditions of the Creative Commons Attribution (CC BY) license (<https://creativecommons.org/licenses/by/4.0/>).

**Abstract:** This work reports the preparation of amino acid-functionalized CQDs from citric acid by facile hydrothermal synthesis. The prepared N-doped CQDs exhibited excellent optical, physical, and chemical properties, and the differences were observed among the six different amino acids used as nitrogen dopants (Leu, Trp, Lys, Arg, Ala, His). Compared to the blank sample (without the addition of amino acids), N-doped CQDs have shown significantly higher quantum yield, also demonstrating the potential in metal ion sensing. The highest quantum yield of 36.45%, with a peak excitation/emission of 340/406 nm, was achieved using citric acid and amino acid Leu (CQD@Leu), treated at temperature of 180 °C during 9 h. The prepared samples were investigated toward metal ion selectivity (Ca<sup>2+</sup>, Cu<sup>2+</sup>, Fe<sup>3+</sup>, K<sup>+</sup>, Hg<sup>2+</sup>, Mg<sup>2+</sup>, Al<sup>3+</sup>, Mn<sup>2+</sup>, and Na<sup>+</sup>), and the CQD@Leu showed a selective and sensitive response upon the addition of Fe<sup>3+</sup> ions. Therefore, CQD@Leu was selected for further investigation in Fe<sup>3+</sup> detection in the model system and real well water samples. A developed model was described by a logistic function with a good coefficient of determination of  $R^2 = 0.9982$ , while the linear range was determined in the concentration range from 0.3 mol dm<sup>-3</sup> to 30 mol dm<sup>-3</sup>, with a determined limit of detection of  $LOD = 1.77 \pm 0.01$  mol dm<sup>-3</sup> and limit of quantification of  $LOQ = 5.89 \pm 0.04$  mol dm<sup>-3</sup>. Furthermore, the results of the in vitro cytotoxicity test (MTT) with normal and tumor cell lines (MRC-5, HeLa, NCI-H358, and CaCo-2) clearly demonstrate the excellent biocompatibility of CQD@Leu.

**Keywords:** carbon quantum dots; citric acid; amino acids; Fe<sup>3+</sup> detection; biocompatibility

## 1. Introduction

Photoluminescent carbon quantum dots (CQDs) have emerged as one of the novel classes of carbon nanomaterials, gradually gaining attention in various industrial and scientific fields in recent years. In general, CQDs are defined as zero-dimensional nanoparticles known for their small sizes, photostability, and outstanding physico-chemical and optical properties [1,2], which enables the widespread applicability of luminescent nanoparticles in biosensing [3–6], chemical sensing [7–14], bioimaging [15,16], photocatalysis [17–20], and biomedicine [15,21–24]. The potential solubility of CQDs in water, their biocompatibility, photostability, high photoluminescence, and facile tunability could provide

an environmentally-friendly alternative to semiconductor quantum dots in theranostics [25–29]. Various different synthetic approaches for the CQDs preparation have been reported, namely “top-down” and “bottom-up” synthetic approaches [30–33]. Recently, the “bottom-up” approach has been gaining significant attention, due to the possibility of obtaining CQDs derived from natural resources and relatively facile surface modification, also conforming principles of green chemistry [34,35]. The CQDs could be synthesized from carbon-containing compounds, most commonly citric acid, [36–41], glucose [42–44], urea [45,46], polyethylene glycol (PEG) [47,48], L-ascorbic acid [43,49], and amino acids [50] are used as precursors for obtaining highly luminescent CQDs. These carbon sources are widespread available, as well as cheap, green, and non-toxic. The determination of optical parameter of quantum yield (QY) is essential, as it defines the photoluminescence efficiency, and finally, the applicability of CQDs in bioimaging and in sensing. This parameter directly determine the image resolution and brightness in cellular imaging; however, the interplay between the various factors, such as emission maximum and photostability, has the major role in determining potential application in diagnostics [21,51]. Additionally, it is well-known that higher QY greatly enhances the sensitivity of photoluminescent nanoprobe for the sensing of different chemical species [52]. Therefore, the preparation of CQDs exhibiting higher QY is the study of interest, bringing new opportunities for sensitive detection using CQDs as photoluminescent nanoprobe. The optoelectronic properties of CQDs could be improved by surface passivation and heteroatom doping, which leads to the increase in surface-state defects creating reactive groups on the surface of nanoparticles [53]. These groups form a thin protective layer that shields CQDs from impurities adhesion and, therefore, improves fluorescence properties [53].

In general, nitrogen-doped (*N*-doped) CQDs are commonly used for sensing purposes, as nitrogen possesses an atomic size similar to the carbon atom, exhibiting strong binding ability and great optical performance of prepared CQDs [54,55]. The rich content of nitrogen in amino acids makes those groups of biomolecules encouraging precursors for obtaining highly luminescent *N*-doped CQDs. In the study by Liu et al. [56], the orbital energy levels involved in *N*-CQDs were investigated by using DFT theoretical calculations. The results have shown that, after introducing *N*-doping to the CQDs, the bandgap energy decreases from 2.01 to 0.64 eV, which could enhance the fluorescence exhibited by *N*-doped CQDs.

It is well-known that iron imbalance homeostasis may cause a variety of health disorders and medical conditions, such as iron deficiency (anemia), hemochromatosis, and neurodegenerative disease (e.g., Alzheimer’s disease, Parkinsonism) [57,58]. Hence, detecting ferric ( $\text{Fe}^{3+}$ ) ions is of great importance for biological systems, as it plays a crucial role in the biochemical pathways of living cells. In general, colorimetric assays and inductively coupled plasma mass spectrometry (ICP-MS) are two of the standard methods for iron detection in biological samples, such as in the blood and urine [59]; however, there is a constant search for novel, inexpensive, facile, and sensitive methods as an efficient alternative.

This study is focused on the amino acid-functionalized CQDs obtained from citric acid by facile hydrothermal synthetic approach. In order to compare the properties and applicability, five amino acids of different chemical complexities (Leu, Trp, Arg, Ala, His) have been used in synthetic procedure, including a blank sample. Differences among the structural, physico-chemical, and optical properties were observed, and the best-performing CQDs sample was tested toward metal ion sensing, both in the model and real samples of well water. In order to investigate potential applications in biomedical analysis, the best-performing sample was tested on the cell viability in both normal and tumor cell lines (MRC-5, HeLa, NCI-H385, CaCo-2, D54). These findings could provide a broader insight into the influences of different amino acid on the CQDs properties and also applicability in the chemical sensing and biomedical analysis.

## 2. Materials and Methods

### 2.1. Chemicals and Materials

All solutions used in experiments were prepared from analytical grade chemicals. Citric acid was supplied by Gram Mol (Zagreb, Croatia), while five different amino acids were purchased as follows: L-leucine (Leu; Kemika, Zagreb, Croatia), L-tryptophan (Trp; Sigma-Aldrich, St. Louis, MO, USA), L-arginine (Arg; Merck, Germany), L-alanine (Ala; Sigma-Aldrich, St. Louis, MO, USA), and L-histidine (His; Sigma-Aldrich, St. Louis, MO, USA). The ultrapure water used in experiments and analysis was obtained by the Milli-Q Millipore system (conductivity  $\leq 0.054 \mu\text{S}/\text{cm}$ ), and it was used for the analytical measurements and sample preparation. Solvents and chemical also used in experiments were acetic acid, acetone, dimethyl sulfoxide (DMSO), ethanol, hydrochloric acid, methanol, and sulfuric acid were supplied by Merck, Germany, while NaOH pellets were purchased by Gram Mol, Croatia. For the purposes of sample purification, dialysis procedure was applied with dialysis membranes Spectra/Por 7 (MWCO 1kDa; Spectrum Labs, Rancho Dominguez, CA, USA). The investigation of the CQDs toward metal ion selectivity was performed with following inorganic salts:  $\text{CaCl}_2 \cdot 2\text{H}_2\text{O}$  (BDH Prolabo, Poole, UK),  $\text{CuCl}_2 \cdot 2\text{H}_2\text{O}$  (Kemika, Croatia),  $\text{FeCl}_3 \cdot 6\text{H}_2\text{O}$  (VWR International, Radnor, PA, USA), KCl (Gram Mol, Croatia),  $\text{HgCl}_2$  (VWR International, USA),  $\text{MgCl}_3 \cdot 6\text{H}_2\text{O}$  (T.T.T., Veliko Trgovišće, Croatia),  $\text{AlCl}_3 \cdot 6\text{H}_2\text{O}$  (Brend Kraft, Duisburg, Germany),  $\text{MnCl}_2 \cdot 4\text{H}_2\text{O}$  (Sigma-Aldrich, St. Louis, MO, USA), and NaCl (Gram Mol, Zagreb, Croatia).

### 2.2. Preparation of Undoped and N-doped CQDs

Undoped and N-doped CQDs were prepared by hydrothermal synthesis, following the procedure of 1000 mg citric acid dissolved in 20 mL of Milli-Q water, and the resulting solution was transferred to a 50 mL of Teflon-lined stainless-steel autoclave (Parr Instrument Company, Moline, IL, USA) and heated up to  $180^\circ\text{C}$  for 9 h in an air oven, in order to obtain pure CQDs, marked as CQD@Blank. The synthesis of N-doped CQDs was carried out by dissolving 175 mg of amino acids in 5 mL of Milli-Q water, and the reaction mixture was further suspended with ultrasound ( $t = 15 \text{ min}$ ; Elmasonic P 70 H, Elma, Siegen, Germany), and then 15 mL of water suspended amino acid was added to the citric acid solution for the overall of 20 mL of reaction mixture. The mixture was transferred to Teflon-lined autoclave and heated at  $180^\circ\text{C}$  for 9 h in an air oven. A total of five N-doped CQDs syntheses were performed using amino acids: Leu (MW = 131.17 g/mol), Trp (MW = 204.23 g/mol), Arg (MW = 174.20 g/mol), Ala (MW = 89.09 g/mol), and His (MW = 155.15 g/mol). Lastly, the prepared CQDs were centrifuged at 10,000 rpm, filtered via Nylon syringe filter ( $0.2 \mu\text{m}$  pore; Agilent Technologies, Palo Alto, CA, USA), and dialyzed against Milli-Q water for 24 h. After the dialysis, purified samples of CQDs were stored in a dark and cool place at  $4^\circ\text{C}$ . Additionally, for further studies, dispersions of CQDs were evaporated by vacuum concentrator (SpeedVac, Savant™ SpeedVac™, Thermo Fisher Scientific, Waltham, MA, USA) or dried by lyophilization process.

### 2.3. Quantum Yield (QY) Measurements

The calculation and determination of quantum yield (QY) was performed according to the procedure described by Alam et al., 2015 [60], and Šafranko et al., 2021 [9]. The absorbance of as-prepared CQDs suspended in water was maintained at  $<0.1$ , in order to minimize the reabsorption effect, and QY was calculated according to Equation (1):

$$\varphi_{\text{CQD}} = \varphi_{\text{QS}} \left[ \frac{I_{\text{CQD}}}{A_{\text{CQD}}} \right] \left[ \frac{A_{\text{QS}}}{I_{\text{QS}}} \right] \left[ \frac{\eta_{\text{CQD}}^2}{\eta_{\text{QS}}^2} \right] \quad (1)$$

where symbol  $\varphi$  represents parameter of quantum yield,  $I$  integrated fluorescence intensity under emission spectrum,  $A$  represents absorbance at the applied excitation wavelength, and  $\eta$  designates the refractive index (1.33 for aqueous solutions). The subscript “CQD” designates the samples of carbon quantum dots, while “QS” refers to the reference quinine

sulfate. The standard solution of quinine sulfate was prepared by dissolving quinine sulfate in 1 L of 0.1 mol dm<sup>-3</sup> of H<sub>2</sub>SO<sub>4</sub> (QY = 0.54 at 360 nm,  $\eta = 1.33$ ) [61]. The results are measured in duplicates and are presented as average values  $\pm$  standard deviations.

#### 2.4. Material Characterization

The optical characterization of the prepared CQDs samples was performed using Cary Eclipse Fluorescence Spectrophotometer (Varian Inc. Santa Clara, CA, USA), while the UV-Vis absorbance measurements were carried out on the uniSPEC 2 spectrophotometer (LLG Labware, Turnov, Czech Republic). Fourier-transform infrared spectroscopy-attenuated total reflectance (FTIR-ATR) analysis was performed using Cary 630 FTIR spectrometer (Agilent technology, Santa Clara, CA, USA), in order to record IR spectra of prepared CQDs. The IR spectra analyses were carried out from 4000 to 600 cm<sup>-1</sup> at a resolution of 4 cm<sup>-1</sup>.

Powder X-ray diffraction patterns were collected on a PANalytical Aeris Research Diffractometer in  $\theta$ - $\theta$  geometry (Malvern PANalytical, Malvern, UK), using CuK $\alpha$  radiation ( $\lambda = 0.1541$  nm, 40 kV, 15 mA) at 298 K. The range of  $2\theta$  was from 20°–80°, with a step size of 0.005°, and counts were collected for 0.25 s at each step. The morphological properties of CQD@Leu were analyzed by high-resolution transmission electron microscopy (HR-TEM) using a JEOL JEM 2200FS FEG HR instrument (JEOL Ltd., Tokyo, Japan) operating at a 200-kV accelerating voltage, and for the CQD@Leu sample, size distribution was determined using JEM -1200EX II (JEOL Ltd., Tokyo, Japan) operating at an 80-kV accelerating voltage. The chemical composition of CQDs was detected by the dispersive X-Ray spectroscopy (EDS, XFlash 6-30, Bruker, Berlin, Germany) attached to scanning electron microscope (SEM, Tescan Vega3 LMU, Fuveau, France). The 200  $\mu$ L of as-prepared samples was drop-coated on Si substrate and dried on a hotplate at 40 °C.

The zeta ( $\zeta$ -) potential of particles suspended in Milli-Q water was determined by dynamic electrophoretic light scattering (ELS) using a photon correlation spectrophotometer (Zetasizer Nano ZS, Malvern Instruments, Worcestershire, UK) equipped with a 532 nm “green” laser. From the measured electrophoretic mobility, zeta potential was calculated by Henry equation using the Smoluchowski approximation. Data were processed using Zetasizer Software 7.13 (Malvern Instrument Worcestershire, UK). Each measurement was repeated three times. All measurements were performed at 25.0  $\pm$  0.1 °C.

#### 2.5. Biocompatibility Tests of CQD@Leu on Tumor and Normal Cells In Vitro

The tested CQD@Leu was dissolved in high-purity water at a concentration of 2 mg mL<sup>-1</sup> as a stock solution, which was used to prepare the final concentrations of 50, 100, 150, and 200  $\mu$ g/mL for the experiments.

The experiments were performed on one normal and three human tumor cell lines: human cervical adenocarcinoma (HeLa), human colorectal adenocarcinoma (CaCo-2), human non-small cell lung cancer (NCI-H358), and human fetal lung fibroblasts (MRC-5). All used cell lines were purchased from ATCC. Cells growing in monolayer were cultured in DMEM (Dulbecco’s modified Eagle medium, Gibco, Thermo Fisher Scientific Inc., Waltham, MA, USA), and for the cells growing in suspension, RPMI 1640 (Gibco, Thermo Fisher Scientific Inc., UK) was used. Media were supplemented with 2 mM glutamine, 10% heat-inactivated fetal bovine serum (FBS, Gibco, Thermo Fisher Scientific Inc., Waltham, MA, USA), and antibiotics (100 U of penicillin and 0.1 mg of streptomycin). The RPMI 1640 was further supplemented with 10 mM HEPES and 1 mM sodium pyruvate. The cells were grown in a CO<sub>2</sub> incubator (IGO 150 CELLlife™, JOUAN, Thermo Fisher Scientific, Waltham, MA, USA) under 37 °C and 5% CO<sub>2</sub> in a humidified atmosphere.

Antiproliferation capacity of CQD@Leu was performed by a slightly modified procedure of the National Cancer Institute [62]. In brief, the cells were plated in 96-well flat bottom plates (Greiner, Frickenhausen, Austria) at a concentration of 2  $\times$  10<sup>4</sup> cells/mL. Twenty-four hours later, the cells were treated with CQD@Leu and incubated for a further 72 h. After incubation, the cell growth rate was evaluated by performing the MTT assay [63]. The absorbance (OD, optical density) was measured on a microplate reader (iMark, BIO

RAD, Hercules, CA, USA) at 595 nm. The percentage of live cells was calculated as follows: % =  $\frac{\text{OD (sample)} - \text{OD (background)}}{\text{OD (control)} - \text{OD (background)}} \times 100$ .

The optical density (OD) of the background is the OD of the MTT solution and DMSO, regarding the cells grown without the tested sample.

### 2.6. Measurements for Selective and Sensitive Metal Detection

To assess whether the prepared CQDs were effective as fluorescent nanoprobe for ion sensing, their selectivity and detection on a total of nine metal ions were investigated:  $\text{Ca}^{2+}$ ,  $\text{Cu}^{2+}$ ,  $\text{Fe}^{3+}$ ,  $\text{K}^+$ ,  $\text{Hg}^{2+}$ ,  $\text{Mg}^{2+}$ ,  $\text{Al}^{3+}$ ,  $\text{Mn}^{2+}$ , and  $\text{Na}^+$ . By dissolving the corresponding metal salts in Milli-Q water, all metal ion stock solutions ( $100 \mu\text{mol dm}^{-3}$ ) were prepared. Stock solutions of CQDs with a concentration of  $25 \mu\text{g mL}^{-1}$  were prepared for the following samples: CQD@Blank, CQD@Leu, CQD@Trp, CQD@Arg, CQD@Ala, and CQD@His. After the samples were concentrated,  $50 \mu\text{L}$  of metal solution was added to  $950 \mu\text{L}$  of CQDs ( $\gamma = 25 \mu\text{g mL}^{-1}$ ) for an overall 1 mL of mixture for the analytical measurements. The reference consisted of 1 mL of as-prepared CQD@Blank sample. Measurements for selective and sensitive metal detection were performed using fluorescence spectroscopy at the excitation wavelength  $\lambda_{\text{EX}} = 340 \text{ nm}$ .

### 2.7. Development of a Model for Detection of $\text{Fe}^{3+}$ Ions Using CQD@Leu

In order to apply the sample CQD@Leu as fluorescent nanoprobe in the quantitative analysis of  $\text{Fe}^{3+}$  ions, mathematical model using logistic function was developed. The procedure included diluting a stock solution of  $\text{Fe}^{3+}$  ions into broad concentration range from 0.01 to  $500 \mu\text{mol dm}^{-3}$  by adding  $100 \mu\text{L}$  of CQD@Leu ( $\gamma = 25 \mu\text{g mL}^{-1}$ ) into the  $900 \mu\text{L}$  of  $\text{Fe}^{3+}$  solution of certain concentration for overall volume of 1 mL. The limit of detection (LOD) and limit of quantification (LOQ) of CQD@Leu toward  $\text{Fe}^{3+}$  ions in a water (model) system were determined according to Equations (2) and (3):

$$\text{LOD} = \frac{3\sigma}{S} \quad (2)$$

$$\text{LOQ} = \frac{10\sigma}{S} \quad (3)$$

where  $\sigma$  designates the standard deviation of  $\text{Fe}^{3+}$  ions concentration and  $S$  is the slope of the calibration curve.

### 2.8. Detection of $\text{Fe}^{3+}$ Ions in Well Water Samples

To further evaluate the efficacy of CQD@Leu on the  $\text{Fe}^{3+}$  ions detection, studies on the model systems and real sample systems were carried out. The real sample systems included three samples of well water, supplied by Veterinary Institute Vinkovci (Vinkovci, Croatia), and water was analyzed according to the standard HRN ISO 6332:1998 method (water quality—determination of iron—spectrometric method using 1,10-phenanthroline). A stock solution of  $\text{Fe}^{3+}$  ions ( $c = 0.01 \text{ mol dm}^{-3}$ ) was prepared by dissolving  $\text{FeCl}_3 \cdot 6\text{H}_2\text{O}$  in Milli-Q water. In all three series of samples,  $990 \mu\text{L}$  CQD@Leu ( $\gamma = 25 \mu\text{g mL}^{-1}$ ) and  $10 \mu\text{L}$  of well water sample (samples designated as 16, 17, and 18) was mixed for overall sample volume of 1 mL. The analysis was performed with well water samples with and without the addition of certain volume ( $200$  or  $400 \mu\text{L}$ ) of stock solution of  $\text{Fe}^{3+}$  ions. After preparation of the samples, measurements were performed using a spectrofluorimetry with excitation wavelength at  $\lambda_{\text{EX}} = 340 \text{ nm}$ .

## 3. Results and Discussion

One-step hydrothermal synthesis was applied to fabricate CQDs from citric acid as a carbon precursor and twelve amino acids (Ala, Arg, Asn, Gln, Glu, Gly, His, Leu, Lys, Phe, Ser i Trp) of different chemical complexities as nitrogen dopants. During the carbonization process, the state of the CQDs surface changes led to the predominant formation of oxygen-

containing groups on the CQDs surface. Additionally, the presence of amino acids induced surface passivation and N-atom incorporation, thus enhancing the properties of prepared CQDs [34]. The results of calculated QY obtained with the addition of corresponding amino acids are presented in Table 1. It has been shown that the CQD@Blank sample obtained without the addition of amino acids exhibited the lowest determined QY of  $QY = (2.02 \pm 1.08)\%$ , while the highest obtained QY was observed in the CQD@Leu sample with  $QY = (36.43 \pm 1.42)\%$  (Figure S1).

**Table 1.** Optical characteristics of the CQDs prepared from citric acid analyzed under pH = 3 and pH = 7.

CQD Sample	N-Dopants	QY/%	$\lambda_{EX}/nm$	$\lambda_{maxEM}/nm$	$\zeta$ -Potential/mV	
					pH = 3	pH = 7
CQD@Leu	Leu	$36.43 \pm 1.42$	340	406	$-5.25 \pm 1.12$	$-47.7 \pm 3.2$
CQD@Trp	Trp	$33.17 \pm 0.85$	365	423	$-0.91 \pm 2.68$	$-24.2 \pm 2.3$
CQD@Arg	Arg	$23.92 \pm 2.11$	335	415	$-12.70 \pm 0.85$	$-14.7 \pm 1.7$
CQD@Lys	Lys	$16.94 \pm 1.94$	335	401	$-13.87 \pm 1.38$	$-16.87 \pm 2.61$
CQD@Ala	Ala	$16.42 \pm 0.77$	340	408	$-5.37 \pm 0.21$	$-15.8 \pm 1.3$
CQD@His	His	$12.97 \pm 2.74$	340	398	$-7.86 \pm 0.94$	$-26.9 \pm 2$
CQD@Gln	Gln	$9.37 \pm 1.71$	340	405	$-9.85 \pm 1.01$	$-9.29 \pm 0.71$
CQD@Ser	Ser	$8.54 \pm 1.96$	340	415	$-5.43 \pm 0.34$	$-14.18 \pm 0.85$
CQD@Asn	Asn	$8.44 \pm 2.39$	340	405	$5.73 \pm 0.25$	$-10.25 \pm 1.12$
CQD@Gly	Gly	$8.13 \pm 3.07$	343	411	$-9.26 \pm 0.26$	$-13.5 \pm 1.43$
CQD@Glu	Glu	$5.75 \pm 1.72$	335	406	$-7.08 \pm 0.26$	$-37.47 \pm 2.18$
CQD@Phe	Phe	$5.11 \pm 2.44$	340	411	$4.17 \pm 0.99$	$-18.92 \pm 2.29$
CQD@Blank	-	$2.02 \pm 1.08$	320	405	$2.18 \pm 1.13$	$-36 \pm 3.4$

Among the all prepared samples of N-CQDs, the lowest QY was determined with sample CQD@Phe with  $QY = (5.11 \pm 2.44)\%$  under pH = 7.

Although there are few publications dealing with the use of N-CQDs in acidic media for heavy metal ion detection [47,64,65], the detection of heavy metals in an acidic environment could induce the hydrolysis of metal ions or exhibit lower fluorescence intensity of N-CQDs. In contrast, in neutral environments, the solubility of certain metal ions, as well as the possibility of precipitation, could be limiting factors in metal ion sensing using N-CQD as a fluorescent nanoprobe [47]. Therefore, the acidic resistance and stability of N-CQDs over the wide range of pH is still a study of interest. In this study, the near-physiological pH = 7 of N-CQDs was used for the sample characterization, investigation of the biocompatibility, and sensing of metal ions.

The surface charge ( $\zeta$ -potential) could be explained based on the known  $pK_a$  values of each individual amino acid used in the synthetic procedures (including also the sample CQD@Blank prepared without the addition of amino acids). The results presented in Table 1 indicate the presence of negative surface charge of  $(-36 \pm 3.4)$  mV for the sample of CQD@Blank under the pH = 7. The citric acid is a tricarboxylic acid having three different  $pK_a$  values, namely 3.15, 4.78, and 6.40 [66], potentially explaining the presence of negative values of  $\zeta$ -potential for the sample CQD@Blank under pH = 7. By assuming that CQD@Blank contains -COOH groups on the surface, at pH = 3, carboxylic groups are protonated, and  $\zeta$ -potential values are shifted toward less negative values  $(-5.25 \pm 1.12)$  mV, compared to the measured  $\zeta$ -potential under pH = 7  $(-36 \pm 3.4)$  mV, where carboxylic groups are assumed to be deprotonated.

By comparing the determined QY and  $\zeta$ -potential values, which indicate the stability of the particles in the suspension, the six best-performing samples were chosen for further analysis: (CQD@Blank;  $QY = 2.02\%$  as reference), CQD@Leu ( $QY = 36.43\%$ ), CQD@Trp ( $QY = 33.17\%$ ), CQD@Arg ( $QY = 23.92\%$ ), CQD@Lys ( $QY = 16.94\%$ ), CQD@Ala ( $QY = 16.42\%$ ), and CQD@His ( $QY = 12.97\%$ ) (Table 1 and Figure 1). From Table 1, it can be seen that the highest QY of  $QY = 36.43\%$  was determined with sample CQD@Leu, while the reference sample CQD@Blank demonstrated the lowest  $QY = 2.02\%$  under pH = 7. The

QY optical parameter is of great importance for determining the applicability of CQDs in fluorescent sensing or cellular imaging [67].

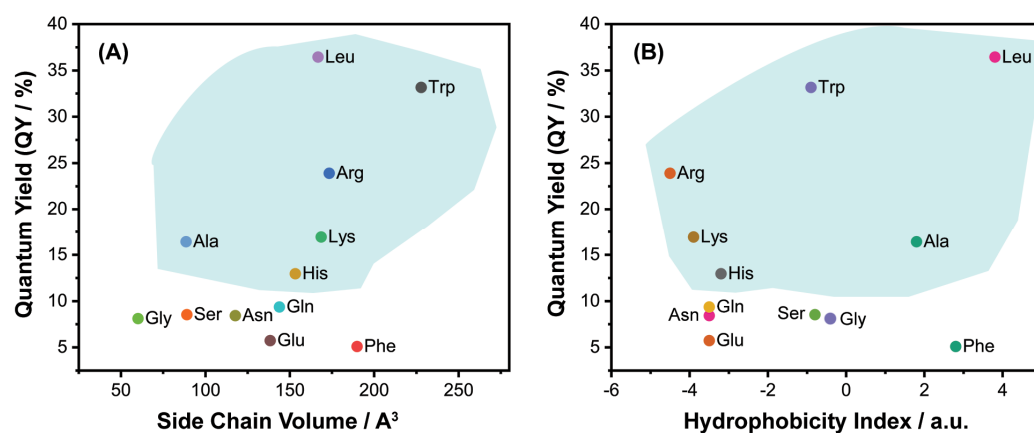


**Figure 1.** The effects of chemical characteristics of amino acids on the determined QY: (A) the effects of side chain volume and (B) the hydrophobicity index. The selected samples of CQDs were marked with blue shadow.

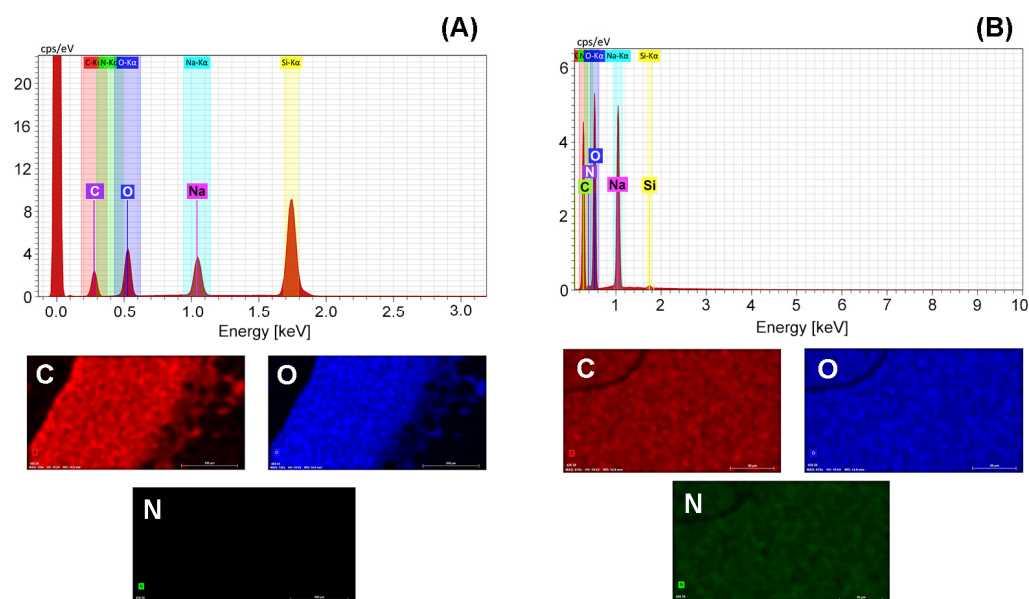
In order to better understand the influence of amino acids on the QY, it is essential to investigate the chemical characteristics of each individual amino acid in detail (Figure 1).

Figure 2 presents the effects of the amino acid's side chain volume and hydrophobicity index on the QY. From the results shown in Figure 1A, the potential increase in QY of the CQDs samples could be a result of the addition of amino acids with greater side chain volume. However, the higher determined QY of sample CQD@Ala, compared to CQD@His, also indicates the potential influence of other factors affecting QY of CQDs. The influence of hydrophobicity index of amino acids on the QY is shown in Figure 1B. The samples of CQDs prepared from hydrophobic amino acids (Trp, Ala, and Leu) showed higher QY values, compared to those prepared from neutral and hydrophilic amino acids. Hence, QY could depend on various factors, and, in this case, it has been shown that synergetic and combining effects of side chain volume and chemical nature of amino acids potentially affect QY [50]. According to Pandit et al. [50], CQDs with hydrophobic amino acids showed higher QY, compared to those with hydrophilic amino acids. The potential explanation was based on the presence of polymeric structure of amino acids, which could produce supramolecular self-assemble structures by hydrophobic interactions, which could also be a key factor for tunable optical properties.

### 3.1. Chemical and Structural Characterization of CQDs

The chemical composition and elemental analysis of selected CQDs was carried out by energy-dispersive X-ray spectroscopy (EDX). The EDX analysis showed the presence of nitrogen content in all prepared *N*-CQDs samples, except in the CQD@Blank sample prepared with citric acid (C<sub>6</sub>H<sub>8</sub>O<sub>7</sub>) and without the addition of amino acid (Table 2). By comparing the parameters of QY and the amount of nitrogen detected by EDX analysis, no significant correlation between these two parameters was observed ( $r = 0.151$ ;  $p < 0.05$ ).

In the study by Liang et al. [68], *N*-CQDs were hydrothermally prepared by using different carbon precursors (xylan, chitosan, soluble starch,  $\beta$ -cyclodextrin) and dopants/passivating agents (NH<sub>4</sub>OH, ethylenediamine, acetic acid). The results demonstrated that CQDs prepared without the addition of dopants/passivating agents exhibited lower QY of 2.06%, while the highest QY of 16.18% showed the CQDs prepared from xylan and 25.0% NH<sub>4</sub>OH, treated at 200 °C during 12 h. A successful nitrogen-doping was achieved by using NH<sub>4</sub>OH as passivation agent forming stable defects on the CQDs surface and enhancing optical properties of CQDs.



**Figure 2.** EDX spectra of (A) CQD@Blank and (B) CQD@Leu.

**Table 2.** Elemental (EDX) analysis of the selected CQDs for the C, O, N elements detection.

CQDs Sample	Mass Weight/%			Atomic Weight/%		
	C/%	O/%	N/%	C/%	O/%	N/%
CQD@Blank	28.31	50.05	-	46.55	35.07	-
CQD@Leu	40.48	46.44	1.60	45.11	38.85	1.53
CQD@Trp	34.31	42.60	3.23	43.19	40.26	3.49
CQD@Arg	37.83	46.14	5.69	42.18	38.62	5.44
CQD@Lys	24.01	30.14	2.04	42.42	39.98	3.09
CQD@Ala	37.22	49.52	3.33	41.18	41.14	3.16
CQD@His	39.82	42.63	6.21	45.50	36.57	6.09

A dispersing ability of CQDs in aqueous media was investigated, and the results are presented in Table 3. The experiments were carried out before and after applying the purification procedure on the CQDs samples. Although there is a statistical significant difference among the samples before and after the purification ( $p = 0.038$ ), these differences are almost negligible. Before purification, the lowest dispersibility showed the sample CQD@Trp with  $(98.46 \pm 0.66)\%$ , while the highest dispersibility in water showed sample CQD@Blank with  $(100.05 \pm 0.50)\%$ . The purification step and determination of the dispersing ability of CQDs is of great importance for applicability evaluation for analytical and biological purposes [69].

**Table 3.** Dispersibility of the prepared CQDs before and after sample purification.

CQDs Sample	Before Purification	After Purification
	Mean Values of Dispersibility/%	
CQD@Blank	$100.05 \pm 0.50$	$99.72 \pm 0.49$
CQD@Leu	$99.00 \pm 1.26$	$99.54 \pm 1.33$
CQD@Trp	$98.46 \pm 0.66$	$99.67 \pm 1.49$
CQD@Arg	$99.56 \pm 0.43$	$99.68 \pm 0.55$
CQD@Lys	$99.74 \pm 0.75$	$99.88 \pm 0.44$
CQD@Ala	$100.04 \pm 0.64$	$100.27 \pm 0.76$
CQD@His	$98.92 \pm 0.55$	$99.80 \pm 1.04$

In addition, the N-CQDs with the highest determined QY, CQD@Leu with QY = 36.43%, was used for further investigation of physicochemical properties. Figure 2 represents the



EDX spectrum with the elemental mapping for the samples CQD@Blank and CQD@Leu. It has been already demonstrated that CQD@Blank (Table 2 and Figure 2A) did not show the presence of nitrogen content in the sample, and the detected nitrogen content in the sample CQD@Leu was  $N\% = 1.53\%$  (Figure 2B). However, from the EDX spectrum, the high content of Na element was detected, probably because of the addition of NaOH for the pH adjustments. This could potentially be explained by the complexation of Na ions with the functional groups on the CQDs surface and the impossibility to remove these ions by dialysis.

The surface charge and stability of CQD@Leu has been investigated by the  $\zeta$ -potential measurements throughout the pH = 2–12 range. It has been also reported that  $\zeta$ -potential could be a useful and efficient method for evaluating the ability of CQDs to adsorb heavy metal ions [70]. The values of the  $\zeta$ -potential of CQD@Leu from pH = 2–12 ranged from  $(3.71 \pm 1.1)$  mV to  $(-65.37 \pm 3.68)$  mV, as shown in Figure 3A. The wider range of the  $\zeta$ -potential values indicated the potential changes in surface charge, probably due to the ionization of functional groups (carboxyl and hydroxyl groups) on the CQDs surface [71]. In an acidic environment under pH = 2, the presence of positive charged particle is detected, probably due to protonation of functional groups present on the CQDs surface. It is also observed that deprotonation is initiated under pH > 3 when the  $\zeta$ -potential decreases. The slight differences are observed in the range of pH = 10–12, indicating the higher stability of CQDs in dispersion. According to Yahaya Pudza et al. [70], at pH greater than pH = 7, stable negatively charged CQDs nanoparticles dominate, leading to the higher affinity of CQDs toward positively charged heavy metals. Moreover, from the  $\zeta$ -potential vs. pH diagram, the isoelectric point ( $\text{pH}_{\text{iep}}$ ) was determined as  $\text{pH}_{\text{iep}} = 2.18$  for the sample CQD@Leu. Additionally, the stability of CQDs in high ionic strength media was investigated under high concentration salt solutions (Figure 3B). The good stability of CQDs in aqueous media is well-known; however, in high concentration salt solutions, there can be tendency of particles to form aggregates, causing a decrease in the fluorescence intensity of CQDs [72]. It has been demonstrated that CQD@Leu nanoparticles have shown excellent stability, even at a very high concentration of  $c(\text{NaCl}) = 1 \text{ mol dm}^{-3}$ , having a negligible effect on the fluorescence emission intensity.

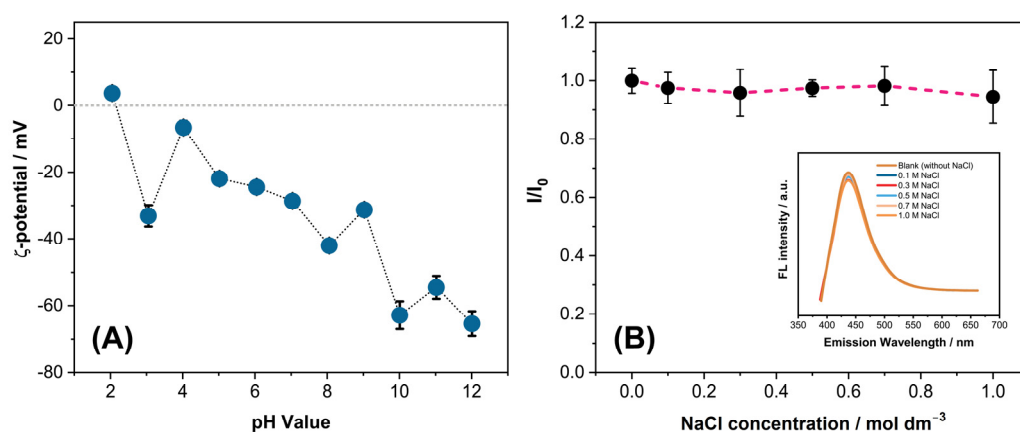


**Figure 3.** CQD@Leu stability studied by (A) variations of  $\zeta$ -potential as a function of pH) and (B) in the high ionic medium of NaCl (0–1.0 mol dm<sup>-3</sup>).

The presence of different functional groups present in the CQD@Blank and CQD@Leu samples has been studied by FTIR spectroscopy (Figure 4). The characteristic broader peaks were detected at  $3267\text{--}3305 \text{ cm}^{-1}$ , indicating the existence of O-H and N-H functional groups. In addition, strong peaks recorded at  $1680 \text{ cm}^{-1}$  and  $1041 \text{ cm}^{-1}$  could be attributed to presence of C=O and C-O vibrations, while the characteristic peak at  $1580 \text{ cm}^{-1}$ ,  $1417 \text{ cm}^{-1}$ ,  $1400 \text{ cm}^{-1}$ , and  $1380 \text{ cm}^{-1}$  potentially indicated the presence of C=C, C-N, and C-O stretching vibrations [71,73]. Along with oxygen-rich functional groups, such as carboxyl, hydroxyl, and carbonyl groups, a presence of amino groups is also detected.

The presence of these functional groups on the CQDs surface could contribute to the good dispersibility of CQDs in aqueous media.

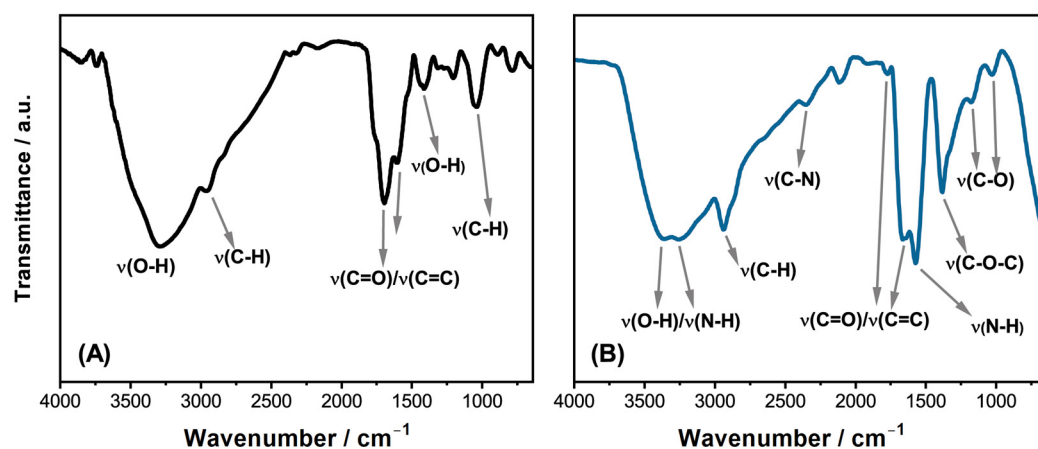


**Figure 4.** FTIR spectra of (A) CQD@Blank and (B) CQD@Leu with corresponding vibrational modes.

Based on the PXRD results (Figure 5), the physical and structural characteristics of CQDs could be described. For the analyzed sample CQD@Leu, the XRD pattern demonstrated the existence of a broad peak centered at  $2\theta = (20.14 \pm 2.84)^\circ$ , which could confirm the amorphous nature of prepared CQDs [71,74]. The calculated interlayer spacing of 0.44 nm for the sample CQD@Leu, compared to 0.34 nm of graphite, indicated and confirmed the presence of amorphous nature and low crystallinity of CQDs, probably caused by surface functionalization [75]. According to the Scherrer equation, the average crystallite size was calculated to be 1.1 nm, while the mean size determined from the TEM images was estimated to be 15.2 nm. These findings indicate that peak broadening presented on the XRD diffractogram could be a result of the presence of amorphous structure.

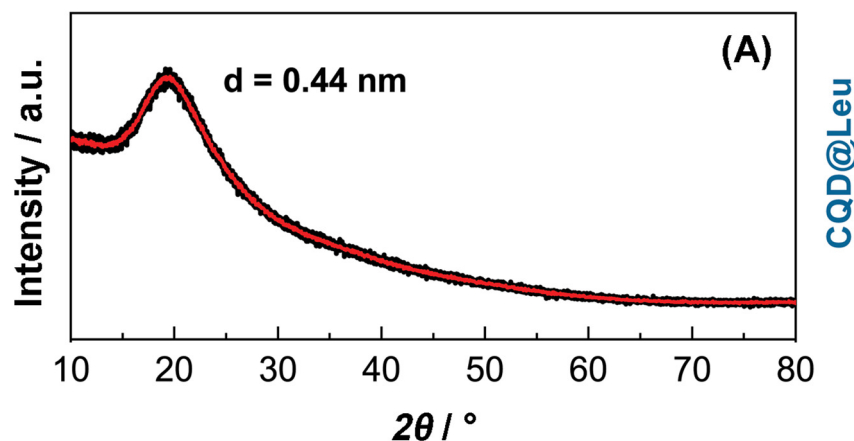


**Figure 5.** XRD pattern of CQD@Leu.

The size and morphological characteristics were studied by TEM techniques. The CQD@Leu nanoparticles TEM images were analyzed to determine the size distribution and the average diameter of 14.38 nm (Figure S2), with a presence of bigger accumulates (Figure S3). The HRTEM image showed a peanut-like shape, hollow structure, and graphite structure on longer sides and amorphous nature on shorter sides of CQD@Leu nanoparticle (Figure S2; inset). It has been reported that the hollow amorphous structures of CQDs could be produced during pyrolysis of carbon sources in the synthetic procedure [76]. Moreover, a number of agglomerates were detected in the sample CQD@Leu, and although the literature mostly defines CQDs as nanoparticles of a size diameter less than 10 nm, there are several studies dealing with CQDs greater than 50 nm [77–79]. It has been reported by

several authors that the size of CQDs depends on the preparation conditions, but also on the storage time and applied purification procedure [77,78].

### 3.2. Optical Characterization of CQDs

In order to evaluate the possible applicability of the prepared CQDs for analytical or biomedical purpose, it is essential to carry out various different studies regarding their optical properties, such as excitation/emission dependence, the influence of different solvents (acetone, DMSO, ethanol, methanol) on the fluorescence intensity, and the effects of pH changes on fluorescence intensity. Due to the lower QY of CQD@Blank (QY = 2.02% under pH = 7), further investigation regarding the influences of solvent and pH are not included. The maximum emission for the CQD@Blank is centered at  $\lambda_{EM} = 405$  nm and excitation wavelength of  $\lambda_{EX} = 320$  nm. The sample with the highest determined QY of QY = 36.43% demonstrated maximum emission at  $\lambda_{EM} = 406$  nm, with excitation wavelength of  $\lambda_{EX} = 340$  nm under pH = 7 (Figure 6A). The maximum emission/excitation wavelengths for other investigated samples are presented in Table 1 and Figure 6.

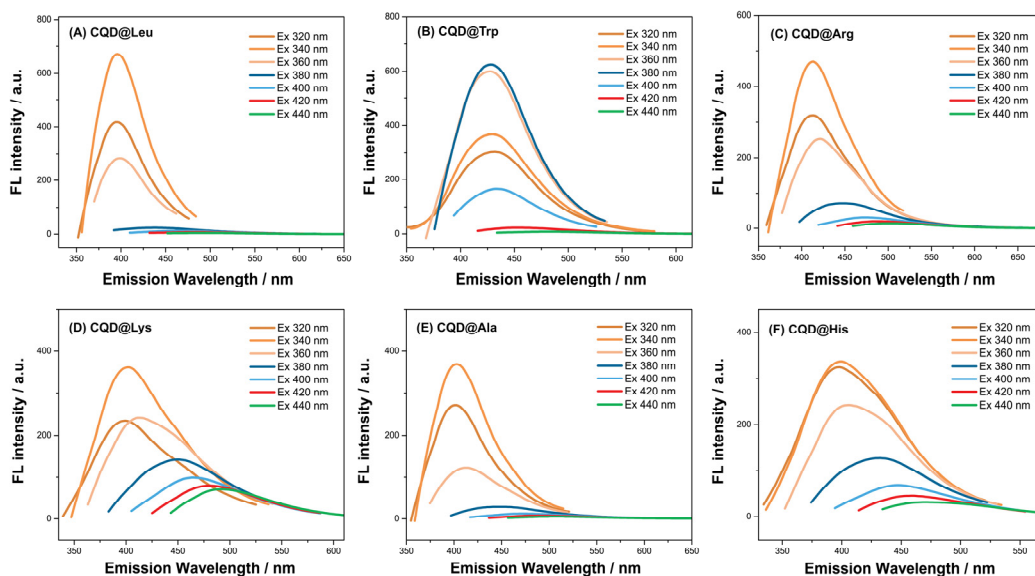


**Figure 6.** Fluorescence spectra of prepared CQDs: (A) CQD@Leu [80], (B) CQD@Trp, (C) CQD@Arg, (D) CQD@Lys, (E) CQD@Ala, (F) CQD@His recorded at different excitation wavelengths ranging from 320 nm to 440 nm (increments of 20 nm).

In order to better understand the impact of different amino acids on the peak position of fluorescence emission spectra of the prepared CQDs, normalized diagrams of the selected CQDs have been provided (Figure 7). The Figure 7 indicates the largest shift of the fluorescence emission of the CQD@Blank toward higher wavelength values (red shift;  $\lambda_{EM} = 445$  nm i  $\lambda_{EM} = 473$  nm). In contrast, all other prepared CQDs showed shifts toward lower wavelengths, showing a lower potential of synthesized CQD for the cellular imaging applications. It is well-known that low QY, short emission wavelength, and complex synthetic and purification procedures could be a limiting factor for the biological and bioanalytical applications [81].

Furthermore, the bandgap values for samples CQD@Blank and CQD@Leu were determined as follows: CQD@Blank with 2.76 eV and CQD@Leu as 3.06 eV. From these results, a consistency with the results shown in Figure 7 can be seen, with the shift of CQD@Blank towards higher emission wavelengths. The proposed energy-level diagrams for both CQD@Blank and CQD@Leu are shown in Figure S4. From the obtained results, it can be seen that *N*-doping potentially induces broadening of the band gap, compared to the undoped CQD@Blank sample. According to the Yang et al. [82], different wavelength shifts are a results of CQD doping, and the hypothesis was confirmed by DFT calculations.

Furthermore, it was reported that even hybridization of molecular orbitals lead to a wider energy gap between the HOMO and LUMO, as well as  $\pi$ - $\pi^*$ , and, in contrast, an uneven distribution can result in a narrower energy gap. In their case, *N*-doping induced a broad band gap in CQDs, while B-doping leads to a narrowing of the band gap in CQDs.

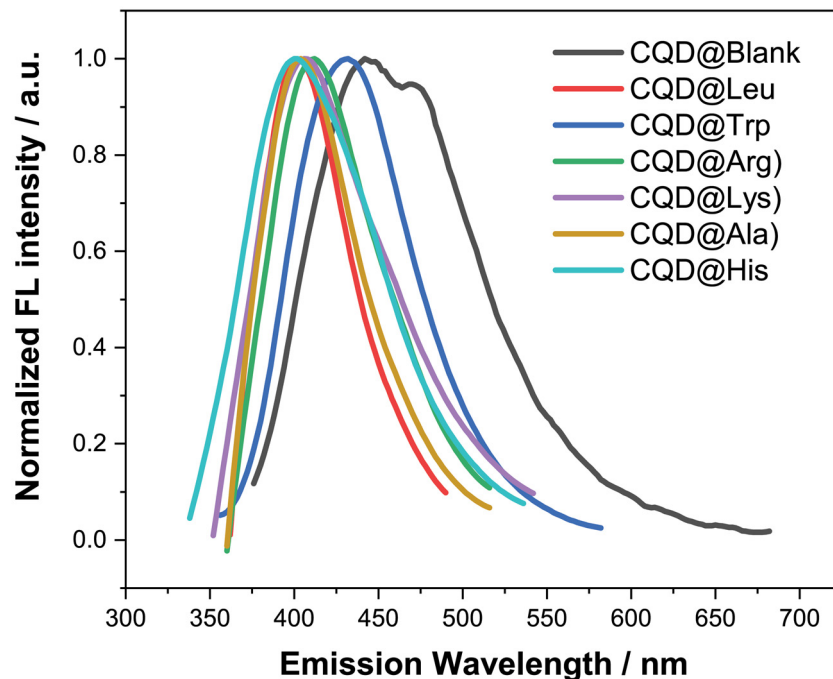


**Figure 7.** The normalized fluorescence intensities for all selected CQDs recorded at  $\lambda_{EX} = 340$  nm.

The influence of the solvents (acetone, DMSO, ethanol, and methanol) on the fluorescence intensity of CQDs has been also studied, as shown in the Figure 8. As it can be seen, the sample CQD@Leu suspended in DMSO, ethanol, and methanol showed similar fluorescence behaviour, while the suspension of CQD@Leu in acetone showed a significant decrease in fluorescence intensity. This means that sample CQD@Leu shows better dispersing ability in polar protic (ethanol, methanol) and polar aprotic (DMSO) solvents.

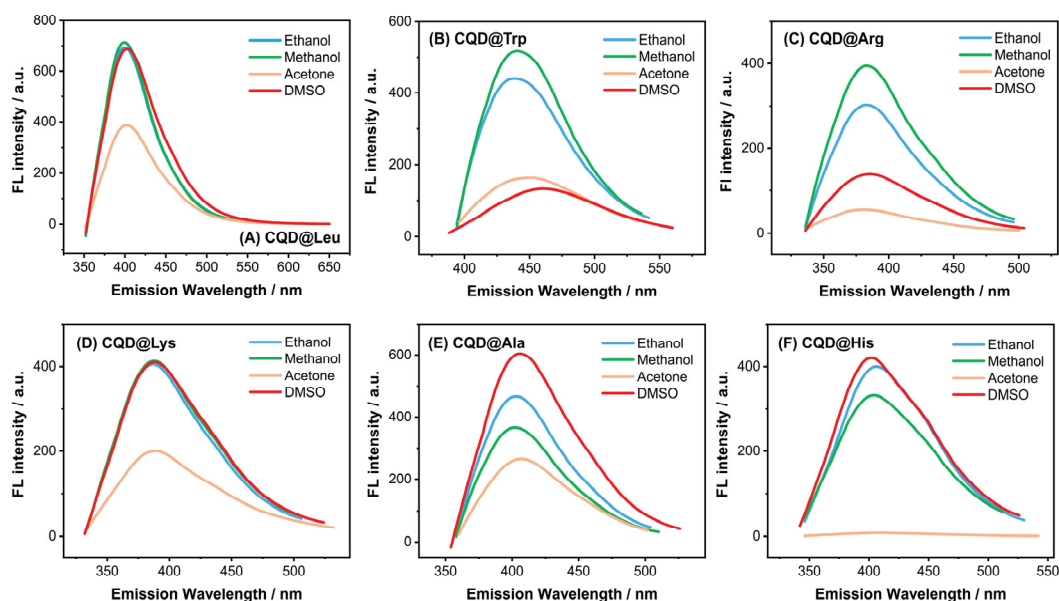


**Figure 8.** Fluorescence spectra of prepared CQDs in different solvents: (A) CQD@Leu, (B) CQD@Trp, (C) CQD@Arg, (D) CQD@Lys, (E) CQD@Ala, (F) CQD@His recorded at  $\lambda_{EX} = 340$  nm.

More pronounced differences were observed with samples CQD@Ala and CQD@His. The highest fluorescence intensity was observed in the dispersion with DMSO, followed by ethanol, methanol, and acetone. This also means a good fluorescence stability of CQDs in the polar aprotic solvent, similar to DMSO; however, the lowest stability has been shown by the acetone, presenting a significant decrease in fluorescence intensity of CQDs. This behaviour of CQDs in different solvents could also be strongly associated with the chemical properties of CQDs and solvents. It is reported that solvent proticity and the ability of forming hydrogen interactions between the functional groups of CQDs and solvents have favorable effects of on the optical properties of CQDs [83,84]. A study by Liu et al. [84] indicates the importance of hydrogen bonding network between the CQDs and protic solvents, which could increase the intramolecular charge transfer effect (from electron donating groups -OH and -NH<sub>2</sub> to electron withdrawing groups -COOH), leading to bigger Stokes' shift in protic solvents.

Furthermore, the effects of pH changes on the CQDs optical stability were investigated (Figure 9). In most analyzed samples, no significant differences were observed in the pH range from pH = 3 to pH = 11, while at the extreme tested pH = 2 and pH = 12, decreases in the fluorescence intensities of the CQDs were observed. As already discussed, in acidic media, the surface charge is shifted toward less negative values, and by increasing the pH of medium, the surface charge appeared to be shifted toward more negative values, indicating the deprotonation of the functional groups on the CQDs surface. There are few studies reporting the important association of the pH medium and changes in fluorescence intensity of CQDs with the ionization of functional groups (carboxyl and hydroxyl groups) on the CQDs surface [64,65].

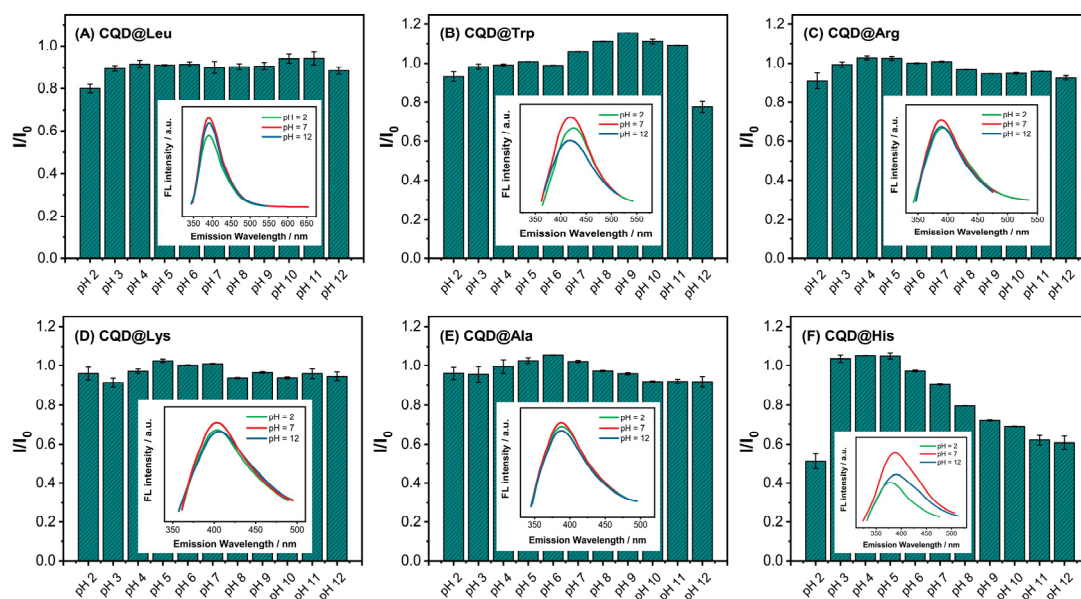


**Figure 9.** Fluorescence intensity vs. pH variation for (A) CQD@Leu, (B) CQD@Trp, (C) CQD@Arg, (D) CQD@Lys, (E) CQD@Ala, (F) CQD@His (recorded at  $\lambda_{EX} = 340$  nm).

Figure 10A shows the UV-Vis spectra of the sample CQD@Leu recorded from 200 nm to 600 nm. It is interesting that the CQDs showed strong absorption in UV region, exhibiting a maximum absorption peak with typical  $\pi-\pi^*$  transition bands, while the absorption peak at 335 nm is attributed to the existence of  $n-\pi^*$  electronic transition of C=O bonds on the CQDs [85]. The 2D contour map also showed the strong absorption in the UV region, and the shape and size of the map could be varied, depending on the applied precursors/dopants, applied synthetic conditions, and solvents used for the synthesis [86].

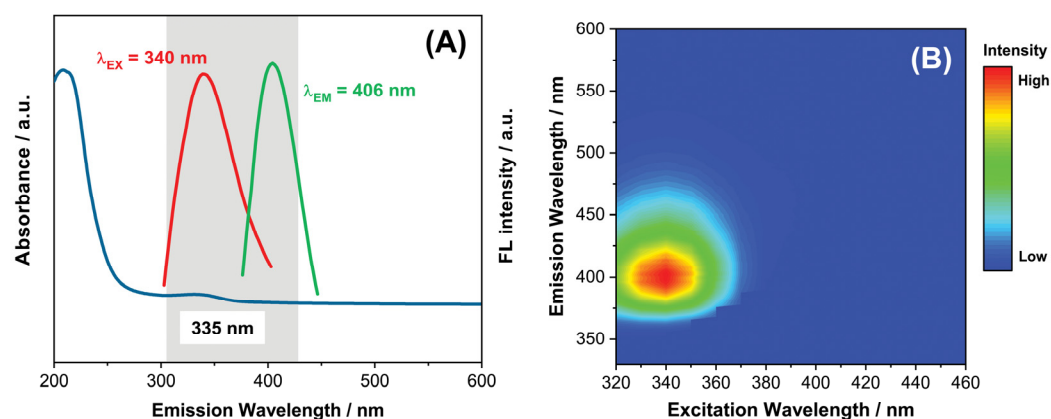


**Figure 10.** (A) UV–Vis absorption spectrum with maximum fluorescence excitation and emission spectrum, and (B) 2D excitation–emission contour map of CQD@Leu [80].

### 3.3. The Application of CQD@Leu in Sensing and $\text{Fe}^{3+}$ Ions Detection

The optical characteristic and stability of CQD@Leu demonstrated a good potential toward establishing a fluorescent nanoprobe for the sensitive and selective detection of metal ions. For the analysis, the selectivity and interference effects in ion sensing and detection were investigated on different metal ions, such as  $\text{Ca}^{2+}$ ,  $\text{Cu}^{2+}$ ,  $\text{Fe}^{3+}$ ,  $\text{K}^+$ ,  $\text{Hg}^{2+}$ ,  $\text{Mg}^{2+}$ ,  $\text{Al}^{3+}$ ,  $\text{Mn}^{2+}$ , and  $\text{Na}^+$ . Firstly, the concentration of CQD@Leu was adjusted to a concentration of  $25 \mu\text{g mL}^{-1}$ , while the concentration of different metal ions was prepared to be  $100 \mu\text{mol dm}^{-3}$ . From the Figure 11, it can be seen that the sample CQD@Leu with the highest determined QY showed a selective response toward the  $\text{Fe}^{3+}$  ions in the model system (the fluorescence intensity  $I$  was reduced to  $>90\%$  compared to blank  $I_0$ ), while the coexistence of other tested metal ions showed a negligible interfering effect on the fluorescence quenching. Furthermore, the samples CQD@Trp and CQD@His have not shown a selective response toward any of the tested ions, compared to the blank sample (without the addition of metal ions). The quenching ability for the sample CQD@Trp was almost identical with ions  $\text{Cu}^{2+}$  (29.96%),  $\text{Fe}^{3+}$  (30.27%), and  $\text{Hg}^{2+}$  (27.05%). Similar behavior was observed with the sample CQD@His, with the ability of quenching of 65.54% for  $\text{Cu}^{2+}$ , 71.04% for  $\text{Fe}^{3+}$ , and 62.19% for  $\text{Hg}^{2+}$  ions. Therefore, the sample CQD@Leu showed the highest and selective affinity toward  $\text{Fe}^{3+}$  ions sensing, and it is further used for the model development, with the purpose of detection of  $\text{Fe}^{3+}$  ions in the model and real sample systems.

Different concentrations of  $\text{Fe}^{3+}$  ions were prepared in the concentration range from  $0.01 \text{ mol dm}^{-3}$  to  $500 \text{ mol dm}^{-3}$ , and the fluorescence spectra is presented in Figure 12A. As above mentioned, the concentration of the CQD@Leu is adjusted to be  $25 \mu\text{g mL}^{-1}$ . The label on the  $y$ -axis  $(I_0 - I)/I_0$  of the Figure 12B represents the ratio of the fluorescence intensity of the blank sample without the addition of  $\text{Fe}^{3+}$  ions ( $I_0$ ), and the intensity determined with samples of different  $\text{Fe}^{3+}$  concentrations ( $I$ ). The fluorescence intensity has gradually reduced with the increase in the  $\text{Fe}^{3+}$  concentration. The relationship between the  $\text{Fe}^{3+}$  concentration and the changes in the fluorescence intensity could be described by logistic function ( $y = 0.0903 - 0.7382/(1 + (x/17.2847)^{0.89})$ ), also showing good fitting with determined coefficient of determination of  $R^2 = 0.9791$  (Figure 12B). The detection limit (LOD) and limit of quantification (LOQ) for the CQD@Leu method toward the  $\text{Fe}^{3+}$  ions detection was calculated to be  $\text{LOD} = (1.77 \pm 0.01) \mu\text{mol dm}^{-3}$  and  $\text{LOQ} = (5.88 \pm 0.04) \mu\text{mol dm}^{-3}$ , within the linear range from  $0.3 \mu\text{mol dm}^{-3}$  to  $30 \mu\text{mol dm}^{-3}$ .

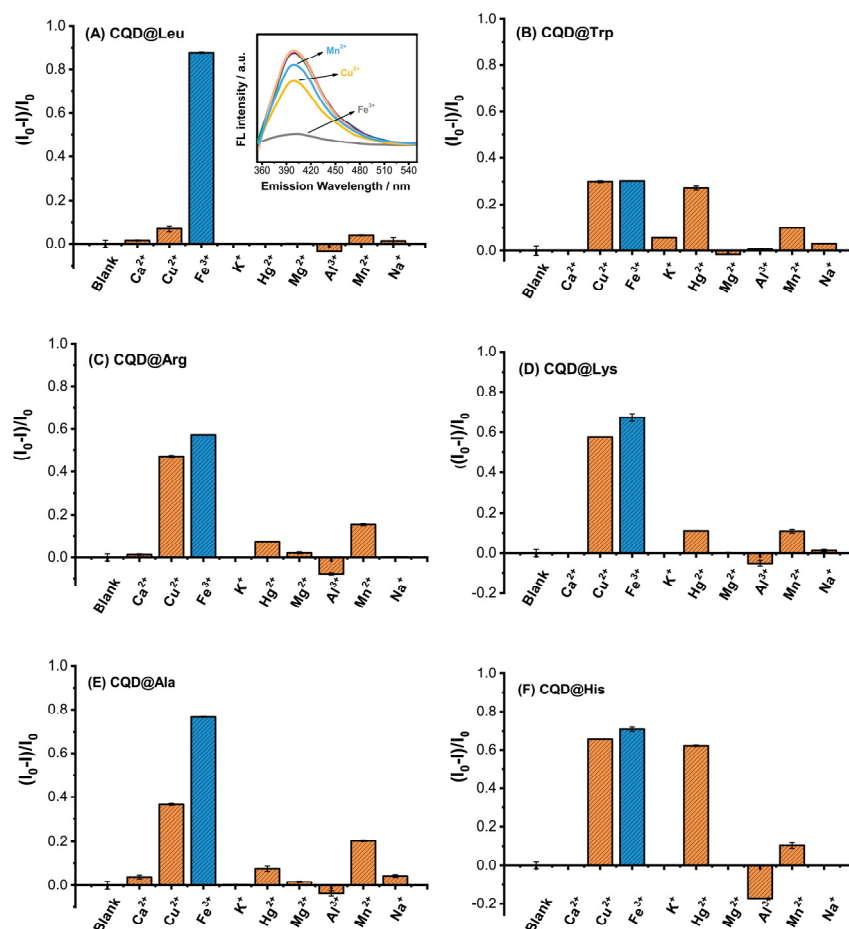


**Figure 11.** Fluorescence response of the samples CQDs to different metal ions: (A) CQD@Leu (inset: fluorescence spectra in the presence of metal ions) [80], (B) CQD@Trp, (C) CQD@Arg, (D) CQD@Lys, (E) CQD@Ala, (F) CQD@His.

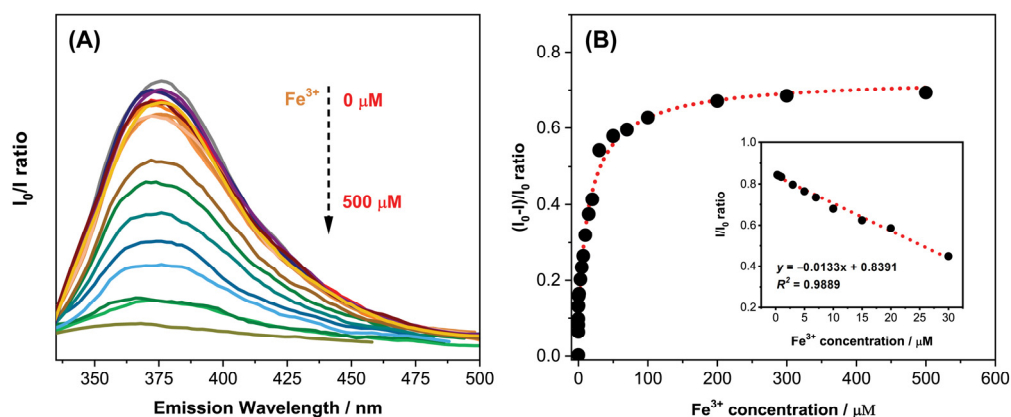


**Figure 12.** (A) Fluorescence intensity of CQD@Leu with various concentrations of  $\text{Fe}^{3+}$  from  $0 \mu\text{mol dm}^{-3}$  to  $500 \mu\text{mol dm}^{-3}$ , and (B) the relative fluorescence response  $(I_0 - I)/I_0$  of CQD@Leu with variations in  $\text{Fe}^{3+}$  concentration [80].

The strong affinity of CQD@Leu toward  $\text{Fe}^{3+}$  ions could be strongly associated with the chemical nature of CQDs. The possible explanation is reported in the study by Zhu et al. [87], emphasizing the possibility of  $\text{Fe}^{3+}$  ions coordinating with the oxygen-rich and amino groups present on the surface of CQDs. Additionally, a more detailed theory is provided by Issa et al. [65], assuming a formation of new bonds between the  $\text{Fe}^{3+}$  ion and functional groups on the CQDs surface, further causing the migration of the electrons in the excited

state to the half-filled *d*-orbitals of Fe<sup>3+</sup>, with an electron configuration of [Ar]3d<sup>5</sup>, which could lead to the fluorescence quenching.

Based on the determined parameters LOD and LOQ, the CQD@Leu sample showed a good potential for the Fe<sup>3+</sup> ions sensing in real sample systems. The investigation in the well water samples was carried out using CQD@Leu as a fluorescent nanoprobe, and the method was evaluated by the standard HRN ISO 6332:1998 (water quality—determination of iron—spectrometric method using 1,10-phenanthroline). The results of the analysis for the detection of Fe<sup>3+</sup> ions using CQD@Leu are presented in Table 4. The method showed high recovery results (97.13–106.14%) with the obtained RSD from 0.85% to 2.89%, also demonstrating satisfactory repeatability and reproducibility. It has been shown that the determined LOD value for the present study is lower than the maximum permissible level (5.36 µM) provided by the World Health Organization for Fe<sup>3+</sup> concentration in drinking water [65], showing a promising potential of a CQD@Leu sensing system for application in real samples.

**Table 4.** Detection of Fe<sup>3+</sup> in real well water samples [80].

Well Water Sample	γ(Fe <sup>3+</sup> ) Determined by Standard Method/µg/L	γ <sub>experimental</sub> (Fe <sup>3+</sup> ) Determined with CQDs Method/µg/L		Mean Value of Fe <sup>3+</sup> Ions in Sample	Recovery <sup>1</sup> /%	RSD/%
		1	2			
16	1338.00	1449.24	1391.08	1420.16 ± 41.12	106.14	2.89
17	2036.00	1965.73	1989.54	1977.63 ± 16.84	97.13	0.85
18	4960.00	5121.45	5048.87	5085.15 ± 51.31	102.52	1.01

<sup>1</sup> Recovery (%) = Amount recovered/starting amount × 100.

The recent literature reporting the application of CQDs prepared from citric acid for the Fe<sup>3+</sup> ions detection with validation parameters is provided in the Table 5.

**Table 5.** Summary of recent published works reporting the application of CQDs prepared from citric acid in Fe<sup>3+</sup> sensing.

Precursors	Linear Range/µM	LOD/µM	Application	References
Citric acid/Phe	5–500	0.73	Detection of Fe <sup>3+</sup> ions in model and real water systems	[88]
Citric acid/ethylenediamine	0–250, 250–1200	1.68	Detection of Fe <sup>3+</sup> ions in model and real water systems	[89]
Citric acid/Phe	0–50	3.5	Detection of Fe <sup>3+</sup> ions in model systems	[37]
Citric acid/ <i>o</i> -phenylenediamine	20–200	1.52	Detection of Fe <sup>3+</sup> ions in model and real water systems	[90]
Citric acid, boric acid and ethylenediamine	2–160	0.08	Detection of Fe <sup>3+</sup> ions in model and real water systems	[91]
Citric acid, polyvinylpyrrolidone, and methionine	1–800	0.00026	Detection of Fe <sup>3+</sup> ions and ascorbic acid	[92]
Citric acid/amino acids (CQD@Leu)	0.3–30	1.77	Detection of Fe <sup>3+</sup> ions in model and real water systems	This work

### 3.4. Cytotoxicity Evaluation of CQD@Leu

To simulate and predict biological responses to CQD@Leu, when applied to or on tissues in the human body, we exposed a normal fibroblast cell line (MRC-5) and three carcinoma cell lines (HeLa, CaCo-2, and NCI-H358) to it at different concentrations for 72 h. As shown in Figure 13, CQD@Leu had no, or a negligible, effect on the growth of both normal and tumor cells at the tested concentrations of 50, 100, 150, and 200 µg/mL. The results obtained clearly demonstrate the excellent biocompatibility of CQD@Leu, with the survival rate of treated cells exceeding 88%, even at the highest concentration applied.



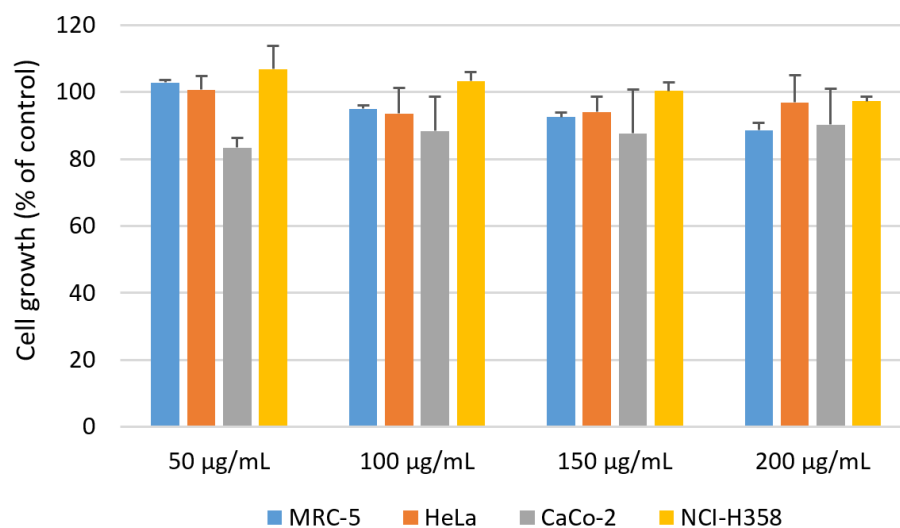


**Figure 13.** The growth-inhibition effect in vitro of CQD@Leu on selected tumor and non-tumor cell lines. Data represents mean values  $\pm$  standard deviation (SD) of three independent experiments. Exponentially growing cells were treated for 72 h. Control cells were non-treated cells. Cytotoxicity was analyzed using MTT survival assay.

#### 4. Conclusions

Highly fluorescent, stable, biocompatible, and water dispersible CQDs have been prepared by simple hydrothermal method using citric acid as a carbon precursor and the amino acids of different chemical complexities. Among the twelve used amino acids, as nitrogen dopants, the six best-performing CQDs with the highest determined QY have been selected for further investigation. The highest QY was determined for the sample CQD@Leu (36.43%), and the lowest QY was exhibited for sample CQD@Blank, prepared without the addition of amino acids under pH = 7. The best-performing sample, CQD@Leu, was studied for physicochemical and optical properties, demonstrating the amorphous nature and spherical morphology of CQD@Leu, with good stability and dispersibility in aqueous medium, while also showing a selective and sensitive response (decrease in the fluorescence intensity) toward  $\text{Fe}^{3+}$  ions. The CQD@Leu nanoparticles were applied as fluorescent nanoprobe for the  $\text{Fe}^{3+}$  ions sensing in model systems, in which a good linear correlation within the  $\text{Fe}^{3+}$  concentration from  $0.3 \mu\text{mol dm}^{-3}$  to  $30 \mu\text{mol dm}^{-3}$  was observed, with determined LOD =  $(1.77 \pm 0.01) \mu\text{mol dm}^{-3}$  and LOQ =  $(5.88 \pm 0.04) \mu\text{mol dm}^{-3}$ . The analysis in real well water samples showed good recovery results (97.13–106.14%) with RSD from 0.85% to 2.89%, compared to a standard method for  $\text{Fe}^{3+}$  ion detection. This work has demonstrated a good potential of N-doped CQDs for  $\text{Fe}^{3+}$  ions sensing, and future investigation could provide new insights and improved strategies for the properties enhancement to further broaden their applicability, especially in the field of biomedical analysis.

**Supplementary Materials:** The following supporting information can be downloaded at: <https://www.mdpi.com/article/10.3390/chemosensors11040205/s1>, Figure S1. Integrated fluorescence intensity vs. absorbance of CQDs samples (recorded at  $\lambda_{\text{EX}} = 360 \text{ nm}$ ); calculated quantum yields (QY) of synthesized samples of CQDs using quinine sulfate as reference standard ( $\varphi_{\text{QS}} = 54\%$ ), Figure S2. TEM images of CQD@Leu; inset: size distribution diagram and HR-TEM image of CQD@Leu, Figure S3. TEM image of CQD@Leu showing amorphous structure of CQDs, Figure S4. The proposed energy-level diagrams for (A) CQD@Blank and (B) CQD@Leu.

**Author Contributions:** Conceptualization, S.Š., S.J.; methodology, S.Š., L.G.O., M.L., Š.M., K.A., M.D.S.; software, S.Š., A.S., (Anamarija Stanković), M.D.S.; validation, S.Š., I.S., S.J.; formal analysis, S.Š., I.S., K.J., M.K., A.S. (Aleksandar Széchenyi), M.D.S.; investigation, S.Š., I.S., K.J., M.K.; data curation, S.Š., I.S., A.S. (Anamarija Stanković), A.S. (Aleksandar Széchenyi), K.A.; writing—original draft preparation, S.Š., S.J., L.G.O., M.L.; writing—review and editing, S.J., I.S., A.S. (Aleksandar Széchenyi), L.G.O.; visualization, S.Š., Š.M., M.D.S., L.G.O., M.L.; supervision, S.J., I.S., A.S. (Aleksandar Széchenyi); funding acquisition, S.J., Š.M. All authors have read and agreed to the published version of the manuscript.

**Funding:** This work has been supported by Croatian Science Foundation, under the project “Application of innovative techniques of the extraction of bioactive compounds from byproducts of plant origin” (UIP-2017-05-9909).

**Institutional Review Board Statement:** Not applicable.

**Informed Consent Statement:** Not applicable.

**Data Availability Statement:** Data are contained within the article.

**Acknowledgments:** This work has been supported by Croatian Science Foundation, under the project “Application of innovative techniques of the extraction of bioactive compounds from byproducts of plant origin” (UIP-2017-05-9909). We also acknowledge the Center of Excellence for Advanced Materials and Sensing Devices (ERDF grant No. KK.01.1.1.01.0001.), and the project supported by the European Union’s Horizon 2020 research and innovation programme under the Marie Skłodowska-Curie grant agreement No 844746 and their working groups for their role in the structural analyses of the samples.

**Conflicts of Interest:** The authors declare no conflict of interest.

## References

1. Mintz, K.J.; Zhou, Y.; Leblanc, R.M. Recent Development of Carbon Quantum Dots Regarding Their Optical Properties, Photoluminescence Mechanism, and Core Structure. *Nanoscale* **2019**, *11*, 4634–4652. [[CrossRef](#)] [[PubMed](#)]
2. Zhang, L.; Yang, X.; Yin, Z.; Sun, L. A Review on Carbon Quantum Dots: Synthesis, Photoluminescence Mechanisms and Applications. *Luminescence* **2022**, *37*, 1612–1638. [[CrossRef](#)]
3. Ji, C.; Zhou, Y.; Leblanc, R.M.; Peng, Z. Recent Developments of Carbon Dots in Biosensing: A Review. *ACS Sens.* **2020**, *5*, 2724–2741. [[CrossRef](#)]
4. Safari, M. Recent Advances in Quantum Dots-Based Biosensors. In *Quantum Dots—Recent Advances, New Perspectives and Contemporary Applications*. *IntechOpen* **2022**. [[CrossRef](#)]
5. Wang, B.; Cai, H.; Waterhouse, G.I.N.; Qu, X.; Yang, B.; Lu, S. Carbon Dots in Bioimaging, Biosensing and Therapeutics: A Comprehensive Review. *Small Sci.* **2022**, *2*, 2200012. [[CrossRef](#)]
6. Qi, C.; Yang, A.; Wang, H.; Zhang, Z.; Wang, J. Ultrasensitive Fluorescent “ON-OFF” Label-Free Immunosensor for Detection of Vitellogenin of Marine Medaka. *Chemosensors* **2022**, *10*, 510. [[CrossRef](#)]
7. Gao, X.; Du, C.; Zhuang, Z.; Chen, W. Carbon Quantum Dot-Based Nanoprobes for Metal Ion Detection. *J. Mater. Chem. C* **2016**, *4*, 6927–6945. [[CrossRef](#)]
8. Chu, H.-W.; Unnikrishnan, B.; Anand, A.; Lin, Y.-W.; Huang, C.-C. Carbon Quantum Dots for the Detection of Antibiotics and Pesticides. *J. Food Drug Anal.* **2020**, *28*, 540–558. [[CrossRef](#)]
9. Šafranko, S.; Goman, D.; Stanković, A.; Medvidović-Kosanović, M.; Moslavac, T.; Jerković, I.; Jokić, S. An Overview of the Recent Developments in Carbon Quantum Dots—Promising Nanomaterials for Metal Ion Detection and (Bio)Molecule Sensing. *Chemosensors* **2021**, *9*, 138. [[CrossRef](#)]
10. Qin, T.; Wang, J.; Liu, Y.; Guo, S. Carbon Quantum Dots Based Chemosensor Array for Monitoring Multiple Metal Ions. *Molecules* **2022**, *27*, 3843. [[CrossRef](#)]
11. Torres Landa, S.D.; Kaur, I.; Agarwal, V. Pithecellobium Dulce Leaf-Derived Carbon Dots for 4-Nitrophenol and Cr(VI) Detection. *Chemosensors* **2022**, *10*, 532. [[CrossRef](#)]
12. Sun, S.; Guo, S.; Qin, Q.; Liao, Y.; Li, M.; Du, F. Box-Behnken Design Optimizing Sugarcane Bagasse-Based Nitrogen-Doped Carbon Quantum Dots Preparation and Application in Ferric Ion Detection. *Chemosensors* **2022**, *10*, 453. [[CrossRef](#)]
13. Guo, Y.; Zhang, L.; Cao, F.; Leng, Y. Thermal treatment of hair for the synthesis of sustainable carbon quantum dots and the applications for sensing Hg<sup>2+</sup>. *Sci. Rep.* **2016**, *6*, 35795. [[CrossRef](#)]
14. Nair, A.N.; Chava, V.S.; Bose, S.; Zheng, T.; Pilla, S.; Sreenivasan, S.T. In situ doping-enabled metal and nonmetal codoping in graphene quantum dots: Synthesis and application for contaminant sensing. *ACS Sustain. Chem. Eng.* **2020**, *8*, 16565–16576. [[CrossRef](#)]

15. Azam, N.; Najabat Ali, M.; Javaid Khan, T. Carbon Quantum Dots for Biomedical Applications: Review and Analysis. *Front. Mater.* **2021**, *8*, 700403. [[CrossRef](#)]
16. Shen, C.-L.; Liu, H.-R.; Lou, Q.; Wang, F.; Liu, K.-K.; Dong, L.; Shan, C.-X. Recent Progress of Carbon Dots in Targeted Bioimaging and Cancer Therapy. *Theranostics* **2022**, *12*, 2860–2893. [[CrossRef](#)] [[PubMed](#)]
17. Fernando, K.A.S.; Sahu, S.; Liu, Y.; Lewis, W.K.; Gulians, E.A.; Jafariyan, A.; Wang, P.; Bunker, C.E.; Sun, Y.-P. Carbon Quantum Dots and Applications in Photocatalytic Energy Conversion. *ACS Appl. Mater. Interfaces* **2015**, *7*, 8363–8376. [[CrossRef](#)] [[PubMed](#)]
18. Heng, Z.W.; Chong, W.C.; Pang, Y.L.; Koo, C.H. An Overview of the Recent Advances of Carbon Quantum Dots/Metal Oxides in the Application of Heterogeneous Photocatalysis in Photodegradation of Pollutants towards Visible-Light and Solar Energy Exploitation. *J. Environ. Chem. Eng.* **2021**, *9*, 105199. [[CrossRef](#)]
19. Domingo-Tafalla, B.; Martínez-Ferrero, E.; Franco, F.; Palomares-Gil, E. Applications of Carbon Dots for the Photocatalytic and Electrocatalytic Reduction of CO<sub>2</sub>. *Molecules* **2022**, *27*, 1081. [[CrossRef](#)] [[PubMed](#)]
20. Zhao, J.; Liu, C.; Li, Y.; Liang, J.; Liu, J.; Qian, T.; Ding, J.; Cao, Y.-C. Preparation of carbon quantum dots based high photostability luminescent membranes. *Luminescence* **2017**, *32*, 625–630. [[CrossRef](#)]
21. Molaei, M.J. Carbon Quantum Dots and Their Biomedical and Therapeutic Applications: A Review. *RSC Adv.* **2019**, *9*, 6460–6481. [[CrossRef](#)] [[PubMed](#)]
22. Su, W.; Wu, H.; Xu, H.; Zhang, Y.; Li, Y.; Li, X.; Fan, L. Carbon Dots: A Booming Material for Biomedical Applications. *Mater. Chem. Front.* **2020**, *4*, 821–836. [[CrossRef](#)]
23. Alaghmandfard, A.; Sedighi, O.; Tabatabaei Rezaei, N.; Abedini, A.A.; Malek Khachatourian, A.; Toprak, M.S.; Seifalian, A. Recent Advances in the Modification of Carbon-Based Quantum Dots for Biomedical Applications. *Mater. Sci. Eng. C* **2021**, *120*, 111756. [[CrossRef](#)] [[PubMed](#)]
24. Adam, G.O.; Sharkar, S.M.; Ryu, J.H. Emerging Biomedical Applications of Carbon Dot and Polymer Composite Materials. *Appl. Sci.* **2022**, *12*, 10565. [[CrossRef](#)]
25. Boakye-Yiadom, K.O.; Kesse, S.; Opoku-Damoah, Y.; Filli, M.S.; Aquib, M.; Joelle, M.M.B.; Farooq, M.A.; Mavlyanova, R.; Raza, F.; Bavi, R.; et al. Carbon Dots: Applications in Bioimaging and Theranostics. *Int. J. Pharm.* **2019**, *564*, 308–317. [[CrossRef](#)]
26. Wang, L.; Choi, W.M.; Chung, J.S.; Hur, S.H. Multicolor Emitting N-Doped Carbon Dots Derived from Ascorbic Acid and Phenylendiamine Precursors. *Nanoscale Res. Lett.* **2020**, *15*, 222. [[CrossRef](#)]
27. Wang, W.; Zhang, Q.; Zhang, M.; Liu, Y.; Shen, J.; Zhou, N.; Lu, X.; Zhao, C. Multifunctional Red Carbon Dots: A Theranostic Platform for Magnetic Resonance Imaging and Fluorescence Imaging-Guided Chemodynamic Therapy. *Analyst* **2020**, *145*, 3592–3597. [[CrossRef](#)]
28. Ross, S.; Wu, R.-S.; Wei, S.-C.; Ross, G.M.; Chang, H.-T. The Analytical and Biomedical Applications of Carbon Dots and Their Future Theranostic Potential: A Review. *J. Food Drug Anal.* **2020**, *28*, 678–696. [[CrossRef](#)]
29. Chen, B.B.; Liu, M.L.; Huang, C.Z. Recent Advances of Carbon Dots in Imaging-Guided Theranostics. *TrAC* **2021**, *134*, 116116. [[CrossRef](#)]
30. Wang, Y.; Hu, A. Carbon Quantum Dots: Synthesis, Properties and Applications. *J. Mater. Chem. C* **2014**, *2*, 6921. [[CrossRef](#)]
31. Bruno, F.; Sciortino, A.; Buscarino, G.; Soriano, M.L.; Ríos, Á.; Cannas, M.; Gelardi, F.; Messina, F.; Agnello, S. A Comparative Study of Top-Down and Bottom-Up Carbon Nanodots and Their Interaction with Mercury Ions. *Nanomaterials* **2021**, *11*, 1265. [[CrossRef](#)] [[PubMed](#)]
32. Khayal, A.; Dawane, V.; Amin, M.A.; Tirth, V.; Yadav, V.K.; Algahtani, A.; Khan, S.H.; Islam, S.; Yadav, K.K.; Jeon, B.-H. Advances in the Methods for the Synthesis of Carbon Dots and Their Emerging Applications. *Polymers* **2021**, *13*, 3190. [[CrossRef](#)] [[PubMed](#)]
33. Cui, L.; Ren, X.; Sun, M.; Liu, H.; Xia, L. Carbon Dots: Synthesis, Properties and Applications. *Nanomaterials* **2021**, *11*, 3419. [[CrossRef](#)]
34. Meng, W.; Bai, X.; Wang, B.; Liu, Z.; Lu, S.; Yang, B. Biomass-Derived Carbon Dots and Their Applications. *Energy Environ. Mater.* **2019**, *2*, 172–192. [[CrossRef](#)]
35. Khairul Anuar, N.K.; Tan, H.L.; Lim, Y.P.; So'aib, M.S.; Abu Bakar, N.F. A Review on Multifunctional Carbon-Dots Synthesized from Biomass Waste: Design/Fabrication, Characterization and Applications. *Front. Energy Res.* **2021**, *9*, 626549. [[CrossRef](#)]
36. Ludmerczki, R.; Mura, S.; Carbonaro, C.M.; Mandity, I.M.; Carraro, M.; Senes, N.; Garroni, S.; Granozzi, G.; Calvillo, L.; Marras, S.; et al. Carbon Dots from Citric Acid and Its Intermediates Formed by Thermal Decomposition. *Chem. Eur. J.* **2019**, *25*, 11963–11974. [[CrossRef](#)]
37. Chahal, S.; Yousefi, N.; Tufenkji, N. Green Synthesis of High Quantum Yield Carbon Dots from Phenylalanine and Citric Acid: Role of Stoichiometry and Nitrogen Doping. *ACS Sustain. Chem. Eng.* **2020**, *8*, 5566–5575. [[CrossRef](#)]
38. Meierhofer, F.; Dissinger, F.; Weigert, F.; Jungclaus, J.; Müller-Caspary, K.; Waldvogel, S.R.; Resch-Genger, U.; Voss, T. Citric Acid Based Carbon Dots with Amine Type Stabilizers: PH-Specific Luminescence and Quantum Yield Characteristics. *J. Phys. Chem. C* **2020**, *124*, 8894–8904. [[CrossRef](#)]
39. Ren, J.; Malfatti, L.; Innocenzi, P. Citric Acid Derived Carbon Dots, the Challenge of Understanding the Synthesis-Structure Relationship. *C* **2020**, *7*, 2. [[CrossRef](#)]
40. Suner, S.S.; Sahiner, M.; Ayyala, R.S.; Bhethanabotla, V.R.; Sahiner, N. Versatile Fluorescent Carbon Dots from Citric Acid and Cysteine with Antimicrobial, Anti-Biofilm, Antioxidant, and AChE Enzyme Inhibition Capabilities. *J. Fluoresc.* **2021**, *31*, 1705–1717. [[CrossRef](#)]

41. Lin, Z.; Zeng, Q.; Deng, Q.; Yao, W.; Deng, H.; Lin, X.; Chen, W. Citric Acid-Derived Carbon Dots as Excellent Cysteine Oxidase Mimics for Cysteine Sensing. *Sens. Actuators B Chem.* **2022**, *359*, 131563. [[CrossRef](#)]
42. Egorova, M.N.; Tomskaya, A.E.; Kapitonov, A.N.; Alekseev, A.A.; Smagulova, S.A. Hydrothermal Synthesis of Luminescent Carbon Dots from Glucose and Birch Bark Soot. *J. Struct. Chem.* **2018**, *59*, 780–785. [[CrossRef](#)]
43. Cailotto, S.; Amadio, E.; Facchin, M.; Selva, M.; Pontoglio, E.; Rizzolio, F.; Riello, P.; Toffoli, G.; Benedetti, A.; Perosa, A. Carbon Dots from Sugars and Ascorbic Acid: Role of the Precursors on Morphology, Properties, Toxicity, and Drug Uptake. *ACS Med. Chem. Lett.* **2018**, *9*, 832–837. [[CrossRef](#)]
44. Lohithakshan, L.C.; Pattarathil, M.S.; Geetha, V.; Kannan, P. Photoluminescent Glucose Derived Carbon Quantum Dots for Photonic and Optoelectronic Applications. In *Proceedings of the OSA Advanced Photonics Congress (AP) 2020 (IPR, NP, NOMA, Networks, PVLED, PSC, SPPCom, SOF), Montreal, QC, Canada, 13–16 July 2020*; Optica Publishing Group: Washington, DC, USA, 2020; p. JT4C.12.
45. Wang, K.; Geng, C.; Wang, F.; Zhao, Y.; Ru, Z. Urea-Doped Carbon Dots as Fluorescent Switches for the Selective Detection of Iodide Ions and Their Mechanistic Study. *RSC Adv.* **2021**, *11*, 27645–27652. [[CrossRef](#)] [[PubMed](#)]
46. Kumar, M.S.; Yasoda, K.Y.; Das, P.; Malik, S.; Kothurkar, N.K.; Batabyal, S.K. Urea-Mediated Synthesized Carbon Quantum Dots to Tune the Electrochemical Performance of Polyaniline Nanorods for Supercapacitor Device. *J. Sci. Adv. Mater. Devices* **2022**, *7*, 100403. [[CrossRef](#)]
47. Qu, F.; Xue, F.; Liu, J.; You, J. Preparation of Carbon Nanodots Capped by Polyethylene Glycol as a Multifunctional Sensor for Temperature and Paracetamol. *Anal. Methods* **2017**, *9*, 4533–4538. [[CrossRef](#)]
48. Peng, Z.; Ji, C.; Zhou, Y.; Zhao, T.; Leblanc, R.M. Polyethylene Glycol (PEG) Derived Carbon Dots: Preparation and Applications. *Appl. Mater. Today* **2020**, *20*, 100677. [[CrossRef](#)]
49. Sugiarti, S.; Darmawan, N. Synthesis of Fluorescence Carbon Nanoparticles from Ascorbic Acid. *Indones. J. Chem.* **2015**, *15*, 141–145. [[CrossRef](#)]
50. Pandit, S.; Behera, P.; Sahoo, J.; De, M. In Situ Synthesis of Amino Acid Functionalized Carbon Dots with Tunable Properties and Their Biological Applications. *ACS Appl. Bio Mater.* **2019**, *2*, 3393–3403. [[CrossRef](#)]
51. Lv, X.; Gao, C.; Han, T.; Shi, H.; Guo, W. Improving the Quantum Yields of Fluorophores by Inhibiting Twisted Intramolecular Charge Transfer Using Electron-Withdrawing Group-Functionalized Piperidine Auxochromes. *Chem. Commun.* **2020**, *56*, 715–718. [[CrossRef](#)]
52. Omar, N.A.S.; Fen, Y.W.; Irmawati, R.; Hashim, H.S.; Ramdzan, N.S.M.; Fauzi, N.I.M. A Review on Carbon Dots: Synthesis, Characterization and its Application in Optical Sensor for Environmental Monitoring. *Nanomaterials* **2022**, *12*, 2365. [[CrossRef](#)] [[PubMed](#)]
53. Dimos, K. Carbon Quantum Dots: Surface Passivation and Functionalization. *COC* **2016**, *20*, 682–695. [[CrossRef](#)]
54. Shah, H.; Xin, Q.; Jia, X.; Gong, J.R. Single Precursor-Based Luminescent Nitrogen-Doped Carbon Dots and Their Application for Iron (III) Sensing. *Arab. J. Chem.* **2019**, *12*, 1083–1091. [[CrossRef](#)]
55. Koç, Ö.K.; Üzer, A.; Apak, R. High Quantum Yield Nitrogen-Doped Carbon Quantum Dot-Based Fluorescent Probes for Selective Sensing of 2,4,6-Trinitrotoluene. *ACS Appl. Nano Mater.* **2022**, *5*, 5868–5881. [[CrossRef](#)]
56. Liu, Y.; Jiang, L.; Li, B.; Fan, X.; Wang, W.; Liu, P.; Xu, S.; Luo, X. Nitrogen doped carbon dots: Mechanism investigation and their application for label free CA125 analysis. *J. Mater. Chem. B* **2019**, *7*, 3053–3058. [[CrossRef](#)]
57. Chung, J.Y.; Kim, H.-S.; Song, J. Iron Metabolism in Diabetes-Induced Alzheimer's Disease: A Focus on Insulin Resistance in the Brain. *Biomaterials* **2018**, *31*, 705–714. [[CrossRef](#)]
58. Takeuchi, H.; Kawashima, R. A Prospective Study on the Relationship between Iron Supplement Intake, Hemoglobin Concentration, and Risk of Parkinsonism. *Nutrients* **2022**, *14*, 4671. [[CrossRef](#)]
59. Stephenson, D.; Nemkov, T.; Qadri, S.M.; Sheffield, W.P.; D'Alessandro, A. Inductively-Coupled Plasma Mass Spectrometry—Novel Insights from an Old Technology into Stressed Red Blood Cell Physiology. *Front. Physiol.* **2022**, *13*, 828087. [[CrossRef](#)]
60. Alam, A.-M.; Park, B.-Y.; Ghouri, Z.K.; Park, M.; Kim, H.-Y. Synthesis of Carbon Quantum Dots from Cabbage with Down- and up-Conversion Photoluminescence Properties: Excellent Imaging Agent for Biomedical Applications. *Green Chem.* **2015**, *17*, 3791–3797. [[CrossRef](#)]
61. Bano, D.; Kumar, V.; Singh, V.K.; Hasan, S.H. Green Synthesis of Fluorescent Carbon Quantum Dots for the Detection of Mercury(II) and Glutathione. *New J. Chem.* **2018**, *42*, 5814–5821. [[CrossRef](#)]
62. Boyd, M.R.; Paull, K.D. Some Practical Considerations and Applications of the National Cancer Institute In vitro Anticancer Drug Discovery Screen. *Drug Dev. Res.* **1995**, *34*, 91–109. [[CrossRef](#)]
63. Mosmann, T. Rapid Colorimetric Assay for Cellular Growth and Survival: Application to Proliferation and Cytotoxicity Assays. *J. Immunol. Methods* **1983**, *65*, 55–63. [[CrossRef](#)] [[PubMed](#)]
64. Chan, K.K.; Yang, C.; Chien, Y.-H.; Panwar, N.; Yong, K.-T. A Facile Synthesis of Label-Free Carbon Dots with Unique Selectivity-Tunable Characteristics for Ferric Ion Detection and Cellular Imaging Applications. *New J. Chem.* **2019**, *43*, 4734–4744. [[CrossRef](#)]
65. Issa, M.A.; Abidin, Z.Z.; Sobri, S.; Rashid, S.A.; Mahdi, M.A.; Ibrahim, N.A. Fluorescent Recognition of Fe<sup>3+</sup> in Acidic Environment by Enhanced-Quantum Yield N-Doped Carbon Dots: Optimization of Variables Using Central Composite Design. *Sci. Rep.* **2020**, *10*, 11710. [[CrossRef](#)]

66. Lambros, M.; Tran, T.; Fei, Q.; Nicolaou, M. Citric Acid: A Multifunctional Pharmaceutical Excipient. *Pharmaceutics* **2022**, *14*, 972. [[CrossRef](#)]
67. Wei, Y.; Chen, L.; Zhao, S.; Liu, X.; Yang, Y.; Du, J.; Li, Q.; Yu, S. Green-Emissive Carbon Quantum Dots with High Fluorescence Quantum Yield: Preparation and Cell Imaging. *Front. Mater. Sci.* **2021**, *15*, 253–265. [[CrossRef](#)]
68. Liang, Z.; Zeng, L.; Cao, X.; Wang, Q.; Wang, X.; Sun, R. Sustainable Carbon Quantum Dots from Forestry and Agricultural Biomass with Amplified Photoluminescence by Simple  $\text{NH}_4\text{OH}$  Passivation. *J. Mater. Chem. C* **2014**, *2*, 9760–9766. [[CrossRef](#)]
69. Li, W.; Wu, S.; Xu, X.; Zhuang, J.; Zhang, H.; Zhang, X.; Hu, C.; Lei, B.; Kaminski, C.F.; Liu, Y. Carbon Dot-Silica Nanoparticle Composites for Ultralong Lifetime Phosphorescence Imaging in Tissue and Cells at Room Temperature. *Chem. Mater.* **2019**, *31*, 9887–9894. [[CrossRef](#)]
70. Yahaya Pudza, M.; Zainal Abidin, Z.; Abdul Rashid, S.; Md Yasin, F.; Noor, A.S.M.; Issa, M.A. Eco-Friendly Sustainable Fluorescent Carbon Dots for the Adsorption of Heavy Metal Ions in Aqueous Environment. *Nanomaterials* **2020**, *10*, 315. [[CrossRef](#)]
71. Sachdev, A.; Gopinath, P. Green Synthesis of Multifunctional Carbon Dots from Coriander Leaves and Their Potential Application as Antioxidants, Sensors and Bioimaging Agents. *Analyst* **2015**, *140*, 4260–4269. [[CrossRef](#)] [[PubMed](#)]
72. Kumari, M.; Chaudhary, G.R.; Chaudhary, S.; Umar, A.; Akbar, S.; Baskoutas, S. Bio-Derived Fluorescent Carbon Dots: Synthesis, Properties and Applications. *Molecules* **2022**, *27*, 5329. [[CrossRef](#)]
73. Li, F.; Rui, J.; Yan, Z.; Qiu, P.; Tang, X. A Highly Sensitive Dual-Read Assay Using Nitrogen-Doped Carbon Dots for the Quantitation of Uric Acid in Human Serum and Urine Samples. *Microchim. Acta* **2021**, *188*, 311. [[CrossRef](#)]
74. Siddique, A.B.; Pramanick, A.K.; Chatterjee, S.; Ray, M. Amorphous Carbon Dots and Their Remarkable Ability to Detect 2,4,6-Trinitrophenol. *Sci. Rep.* **2018**, *8*, 9770. [[CrossRef](#)]
75. Qiang, R.; Yang, S.; Hou, K.; Wang, J. Synthesis of Carbon Quantum Dots with Green Luminescence from Potato Starch. *New J. Chem.* **2019**, *43*, 10826–10833. [[CrossRef](#)]
76. Guo, F.; Zhu, Z.; Zheng, Z.; Jin, Y.; Di, X.; Xu, Z.; Guan, H. Facile Synthesis of Highly Efficient Fluorescent Carbon Dots for Tetracycline Detection. *Environ. Sci. Pollut. Res.* **2020**, *27*, 4520–4527. [[CrossRef](#)] [[PubMed](#)]
77. Stachowska, J.D.; Murphy, A.; Mellor, C.; Fernandes, D.; Gibbons, E.N.; Krysmann, M.J.; Kellarakis, A.; Burgaz, E.; Moore, J.; Yeates, S.G. A Rich Gallery of Carbon Dots Based Photoluminescent Suspensions and Powders Derived by Citric Acid/Urea. *Sci. Rep.* **2021**, *11*, 10554. [[CrossRef](#)] [[PubMed](#)]
78. Javed, N.; O'Carroll, D.M. Long-Term Effects of Impurities on the Particle Size and Optical Emission of Carbon Dots. *Nanoscale Adv.* **2021**, *3*, 182–189. [[CrossRef](#)] [[PubMed](#)]
79. Javed, N.; O'Carroll, D.M. Carbon Dots and Stability of Their Optical Properties. *Part. Part. Syst. Character.* **2021**, *38*, 2000271. [[CrossRef](#)]
80. Šafranko, S.; Janděl, K.; Kovačević, M.; Dutour Sikirić, M.; Mandić, Š.; Széchenyi, A.; Strelec, I.; Jokić, S. Preparation of Amino Acid Functionalized Carbon Quantum Dots from Citric Acid Efficient Fluorescent Nanoprobe for Selective Detection of  $\text{Fe}^{3+}$  Ions in Model Systems and in Well Water Samples (poster presentation). In Proceedings of the 26th International Congress of Chemical and Process Engineering—CHISA 2022—Congress Book, Prague, Czech Republic, 21–25 August 2022.
81. Zhang, X.; Li, S.; Ma, H.; Wang, H.; Zhang, R.; Zhang, X.-D. Activatable NIR-II Organic Fluorescent Probes for Bioimaging. *Theranostics* **2022**, *12*, 3345–3371. [[CrossRef](#)]
82. Yang, G.; Wu, C.; Luo, X.; Gao, Y.; Wu, P.; Cai, C.; Saavedra, S.S. Exploring the Emissive States of Heteroatom-Doped Graphene Quantum Dots. *J. Phys. Chem. C* **2018**, *122*, 11–6483. [[CrossRef](#)]
83. Hu, Y.; Neumann, C.; Scholtz, L.; Turchanin, A.; Resch-Genger, U.; Eigler, S. Polarity, Intramolecular Charge Transfer, and Hydrogen Bond Co-Mediated Solvent Effects on the Optical Properties of Graphene Quantum Dots. *Nano Res.* **2023**, *16*, 45–52. [[CrossRef](#)]
84. Liu, H.; Yang, J.; Li, Z.; Xiao, L.; Aryee, A.A.; Sun, Y.; Yang, R.; Meng, H.; Qu, L.; Lin, Y.; et al. Hydrogen-Bond-Induced Emission of Carbon Dots for Wash-Free Nucleus Imaging. *Anal. Chem.* **2019**, *91*, 9259–9265. [[CrossRef](#)]
85. Wang, M.; Wan, Y.; Zhang, K.; Fu, Q.; Wang, L.; Zeng, J.; Xia, Z.; Gao, D. Green Synthesis of Carbon Dots Using the Flowers of *Osmanthus Fragrans* (Thunb.) Lour. as Precursors: Application in  $\text{Fe}^{3+}$  and Ascorbic Acid Determination and Cell Imaging. *Anal. Bioanal. Chem.* **2019**, *411*, 2715–2727. [[CrossRef](#)] [[PubMed](#)]
86. Das, G.S.; Shim, J.P.; Bhatnagar, A.; Tripathi, K.M.; Kim, T. Biomass-Derived Carbon Quantum Dots for Visible-Light-Induced Photocatalysis and Label-Free Detection of  $\text{Fe(III)}$  and Ascorbic Acid. *Sci. Rep.* **2019**, *9*, 15084. [[CrossRef](#)] [[PubMed](#)]
87. Zhu, J.; Chu, H.; Wang, T.; Wang, C.; Wei, Y. Fluorescent Probe Based Nitrogen Doped Carbon Quantum Dots with Solid-State Fluorescence for the Detection of  $\text{Hg}^{2+}$  and  $\text{Fe}^{3+}$  in Aqueous Solution. *Microchem. J.* **2020**, *158*, 105142. [[CrossRef](#)]
88. Pu, Z.-F.; Wen, Q.-L.; Yang, Y.-J.; Cui, X.-M.; Ling, J.; Liu, P.; Cao, Q.-E. Fluorescent Carbon Quantum Dots Synthesized Using Phenylalanine and Citric Acid for Selective Detection of  $\text{Fe}^{3+}$  Ions. *Spectrochim. Acta A Mol. Biomol. Spectrosc.* **2020**, *229*, 117944. [[CrossRef](#)]
89. Xiang, Z.; Jiang, Y.; Cui, C.; Luo, Y.; Peng, Z. Sensitive, Selective and Reliable Detection of  $\text{Fe}^{3+}$  in Lake Water via Carbon Dots-Based Fluorescence Assay. *Molecules* **2022**, *27*, 6749. [[CrossRef](#)]
90. Bao, W.; Lan, Y.; Lu, H.; Li, G.; Yu, M.; Yang, J.; Wei, L.; Su, Q. A Dual-Function Carbon Quantum Dot Fluorescent Probe for the Detection of  $\text{Fe}^{3+}$  and Sunset Yellow. *ChemistrySelect* **2022**, *7*, e202202375. [[CrossRef](#)]

91. Zhang, Y.; Qin, H.; Huang, Y.; Zhang, F.; Liu, H.; Liu, H.; Wang, Z.J.; Li, R. Highly Fluorescent Nitrogen and Boron Doped Carbon Quantum Dots for Selective and Sensitive Detection of Fe<sup>3+</sup>. *J. Mater. Chem. B* **2021**, *9*, 4654–4662. [[CrossRef](#)]
92. Yang, Z.; Xu, T.; Zhang, S.; Li, H.; Ji, Y.; Jia, X.; Li, J. Multifunctional N,S-Doped and Methionine Functionalized Carbon Dots for on-off-on Fe<sup>3+</sup> and Ascorbic Acid Sensing, Cell Imaging, and Fluorescent Ink Applying. *Nano Res.* **2022**. [[CrossRef](#)]

**Disclaimer/Publisher's Note:** The statements, opinions and data contained in all publications are solely those of the individual author(s) and contributor(s) and not of MDPI and/or the editor(s). MDPI and/or the editor(s) disclaim responsibility for any injury to people or property resulting from any ideas, methods, instructions or products referred to in the content.